

1 Manuscript type: Research article

2 **COMPREHENSIVE LANDSLIDE SUSCEPTIBILITY MAP OF CENTRAL ASIA**

3 Ascanio Rosi^{a,b}, William Frodella^{b,c,*}, Nicola Nocentini^{b,c}, Francesco Caleca^{b,c}, Hans Balder Havenith^d, Alexander
4 Strom^{e,f}, Mirzo Saidov^g, Gany Amirgalievich Bimurzaev^h, Veronica Tofani^{b,c}

5 ^a Department of Geosciences, University of Padua, Via G. Gradenigo 6, 35131, Padua, Italy

6 ^b UNESCO Chair on the Prevention and Sustainable Management of Geo-Hydrological Hazards, University of
7 Florence, Largo Fermi 2, 50125 Florence, Italy

8 ^c University of Florence, Department of Earth Sciences, via G. la Pira 4, 50121 Florence, Italy.

9 ^d Department of Geology, University of Liege, 4000 Liege, Belgium

10 ^e Geodynamics Research Center LLC, Moscow, 125008, Russian Federation

11 ^f Geodynamics Research Center - branch of JSC “Hydroproject Institute”, Moscow, 125993, Russian Federation

12 ^g Institute of Water problems, Hydropower, Engineering and Ecology of Tajikistan (IWPHE), 734063, Dushanbe,
13 Tajikistan

14 ^h State Service of the Republic of Uzbekistan for Geohazards Monitoring, 100074, Tashkent, Uzbekistan

15 * Correspondence: william.frodella@unifi.it; +39 055 2755979

16 **Abstract**

17 Central Asia is an area characterized by complex tectonics and active deformation; the related seismic activity
18 controls the earthquake hazard level that, due to the occurrence of secondary and tertiary effects, has also direct
19 implications on the hazard related to mass movements as landslides, which are responsible for an extensive number
20 of casualties every year. Climatically, this region is characterized by strong rainfall gradient contrasts, due to the
21 diversity of climate and vegetation zones. The region is drained by large, partly snow- and glacier-fed rivers, that
22 cross or terminate in arid forelands; therefore, it is affected also by a significant river flood hazard, mainly in spring
23 and summer seasons. The challenge posed by the combination of different hazards can only be tackled considering
24 a multi-hazard approach harmonized among the different countries, in agreement with the requirements of the
25 Sendai Framework for Disaster Risk Reduction. This work was carried out within the framework of the SFRARR
26 Project (“*Strengthening Financial Resilience and Accelerating Risk Reduction in Central Asia*”) as a part of a
27 multi-hazard approach, and is focused on the first landslide susceptibility analysis at a regional scale for Central
28 Asia. To this aim the most detailed landslide inventories, covering both national and transboundary territories were
29 implemented in a Random Forest model, together with several independent variables. The proposed approach
30 represents an innovation in terms of resolution (from 30 to 70 m) and extension of the analysed area with respect
31 to previous regional landslide susceptibility and hazard zonation models applied in Central Asia. The final aim
32 was to provide a useful tool for land use-planning and risk reduction strategies to landslide scientists, practitioners,
33 and administrators.

34 **1. Introduction**

35 During the two decades spanning between 1988 and 2007, according to observed estimates, out of 177 reported
 36 disasters in Central Asia 13% were landslides, causing 700 deaths (Table 1), while in the same period economic
 37 losses have been as high as \$150 million, including damage to infrastructures, settlements and agricultural/pasture
 38 lands, as well as displacement of the population (GFDRR, 2009). More recent modelled estimates show that in the
 39 Central Asia states an annual average of 3 million persons are affected by earthquakes and floods, with an estimated
 40 annual average GDP of 9 billion USD (GFDRR, 2016).

41 **Table 1: Observed landslide hazard statistics (1988-2007).** Source: Risk assessment for Central Asia and
 42 Caucasus (UN ISDR, 2009).

Country	No. disasters/year	Total no. of deaths	Deaths/year	Relative vulnerability (deaths/year/million)
Kazakhstan	0.05	48	2.40	0.16
Kyrgyz Republic	0.30	238	11.90	2.27
Tajikistan	0.50	339	16.95	2.51
Turkmenistan	n.a.	n.a.	n.a.	n.a.
Uzbekistan	0.15	75	3.75	0.14

43 Due to their large size and impact, most of the occurring landslides have profound transboundary implications.
 44 Tajikistan and Kyrgyz Republic are the countries most impacted by landslides: in Tajikistan around 50000
 45 landslide were mapped, 1,200 of which threaten settlements or facilities (Thurman, 2011), while Kyrgyz Republic
 46 has been affected by 5,000 landslides, of which 3,500 at various levels of activity are located in the southern
 47 portion of the country (the Fergana Valley area) (Pusch, 2004; Li et al., 2021). Only in Kyrgyz Republic, up to
 48 2017, 784 landslides and 1658 mudflows (also including loess flows) and flash floods caused 352 victims
 49 (Kalmetieva et al., 2009; Havenith et al., 2015a; 2017). Almaty province in Kazakhstan, Tashkent, Samarkand,
 50 Surkhandarya, Kashkadarya Provinces of Uzbekistan, and Ahal Province of Turkmenistan are also exposed to
 51 landslides (World Bank, 2006). Given the increased anthropogenic pressures and the impact of climate change,
 52 since the early '90s several projects have tried to improve the knowledge on landslide hazard (Thurman, 2011),
 53 by providing landslide losses estimations, location, type, triggering/reactivation dates, inventories and hazard/risk
 54 maps, as well as platforms to retrieve open disaster risk data and overviews on landslide risk reduction strategies.
 55 Amongst the regional studies on landslide hazard, providing descriptions, statistics, and inventory maps, it is worth
 56 mentioning:

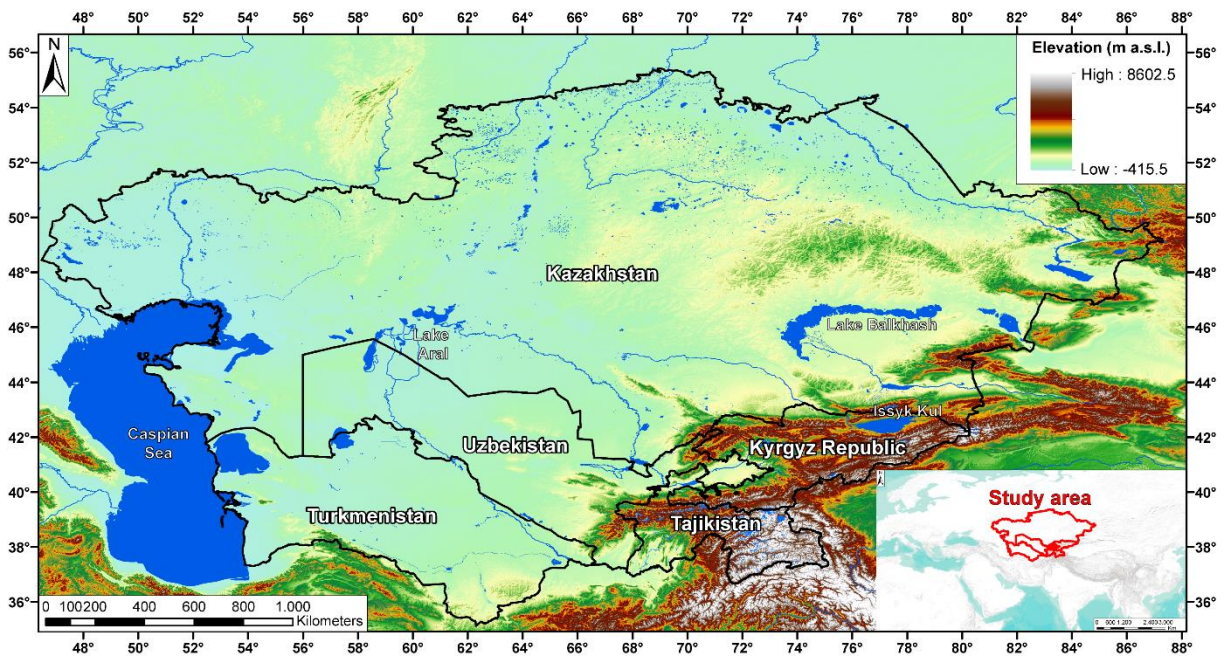
- 57 • Disaster Risk Management and Climate Change Adaptation in Europe and Central Asia, developed by the
 58 World Bank - Global Facility for Disaster Reduction and Recovery (Pollner et al., 2010).
- 59 • Disaster Risk Reduction, 20 Examples of Good Practice from Central Asia, developed by the European Union,
 60 International Strategy for Disaster Reduction ISDR (European Commission Humanitarian Aid, Civil
 61 Protection, 2006).

- 62 • Science for Peace Project (983289) ‘Prevention of landslide dam disasters in the Tien Shan, LADATSHA’.
63 2009–2012, NATO Emerging Security Challenges Division.
- 64 • PROGRESS (Potsdam Research Cluster for Georisk Analysis, Environmental Change and Sustainability).
65 German Federal Ministry of Research and Technology (BMBF).
- 66 • Tian Shan-Pamir Monitoring Program (TIPTIMON). German Federal Ministry of Education and Research
67 (BMBF).
- 68 • M126 IPL Project (funded by the International Consortium on Landslides): M2002111 Detailed study of the
69 internal structure of large rockslide dams in the Tien Shan; M2004126 Compilation of landslide/rockslide
70 inventory of the Tien Shan Mountain System.

71 Besides the creation of landslide inventories, a common approach to assess landslide hazard is the development of
72 landslide susceptibility maps (LSMs), which depict the relative probability of occurrence of a given type of
73 landslide in a given area, without considering the probability of occurrence in time (Brabb, 1984). In other words,
74 LSMs identify those areas where landslides can occur, based on their geological, morphological, and climatic
75 characteristics. These maps have been extensively used as useful tools for land planning (Cascini 2008; Frattini et
76 al., 2010) and hazard assessment (Corominas et al., 2003). More recently, they have been successfully integrated
77 also in quantitative risk assessment (Chen et al., 2016), and early warning systems (Segoni et al., 2018; Tiranti et
78 al., 2019). LSMs have been produced by applying a wide range of mathematical techniques, from the most
79 traditional statistic approaches like frequency ratio (Yilmaz, 2009), discriminant analysis (Carrara, 1983; Trigila
80 et al., 2013) and logistic regression (Lee, 2005; Duman et al., 2006; Manzo et al., 2013), to more recent and more
81 advanced techniques, like artificial neural network (Tien Bui et al., 2016; Ermini et al., 2005), machine learning
82 (Catani et al., 2013) and multi criteria decision analysis (Akgun, 2012). Statistical-probabilistic models for
83 landslide susceptibility can overcome the data gaps and allow to analyse very wide areas (from basin to national
84 scales), by adopting a homogeneous methodology and a harmonized dataset (including global and local data
85 sources). However, landslide hazard assessment is a complex process since it needs accurate knowledge of the
86 topic and appropriate input data (historical inventories, and regional inventories that consist of large prehistoric
87 events mainly). In this work the landslide susceptibility analysis was carried out by means of the “Random Forest”
88 machine learning algorithm, which is credited as one of the most advanced and reliable techniques in this field
89 (Catani et al., 2013, Goetz et al 2015). This work represents the first landslide susceptibility analysis at a regional
90 scale for Central Asia, and was carried out in the framework of the SFRARR Project (“Strengthening Financial
91 Resilience and Accelerating Risk Reduction in Central Asia”) as a part of a multi-hazard approach (Bazzurro et
92 al., in prep). The main challenge of this work was the creation of a unique LSM of the whole Central Asia, that
93 involved the use of a wide range of variables, to account the features of each country, a high volume of input data,
94 and the development of new approaches to analyse these data and to take into accounts possible discrepancies and
95 non-homogeneities. The proposed approach represents an innovation in terms of resolution, extension of the
96 analysed area with respect to previous regional landslide susceptibility and hazard zonation models applied in
97 Central Asia (e.g., Nadim et al., 2006; Havenith et al., 2015b; Stanley and Kirshbaum, 2017; Pittore et al., 2018;
98 World Bank, 2020).

99 **2. Study area**

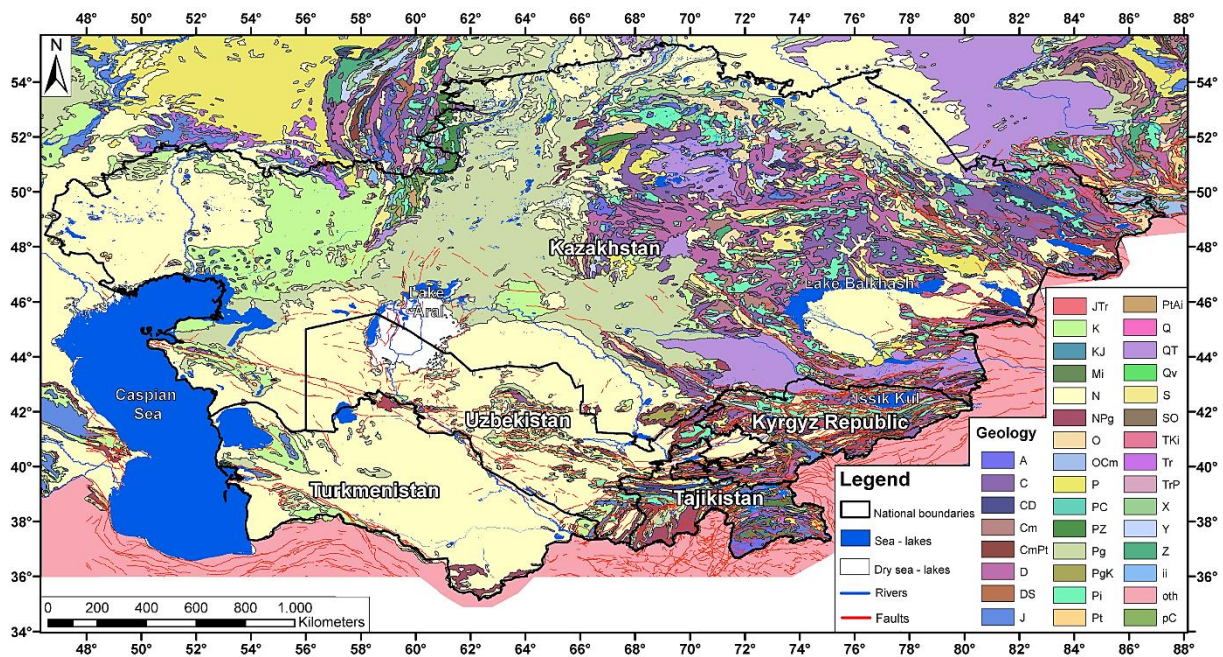
100 Geographically, Central Asia is a vast and diverse region including high mountain chains, deserts, and steppes
 101 (Fig. 1). A large portion of the Central Asia countries, especially the southern and eastern parts of the region, are
 102 occupied by the mountainous areas of the Djungaria, Tien Shan, Pamir, Kopetdag, and small part of Western Altaj,
 103 with peaks above 7,000 m a.s.l (Strom, 2010). These intraplate mountain systems formed in the Cenozoic between
 104 the Tarim Basin and the Kazakh Shield, as a result of the India-Asian collision (Molnar and Tapponier 1975,
 105 Abdrakhmatov et al., 1996; 2003; Zubovich et al., 2010, Ullah et al., 2015). This work is focused in the most inner
 106 part of Central Asia, represented by the territories of Turkmenistan, Kazakhstan, Kyrgyz Republic, Uzbekistan,
 107 and Tajikistan. Active mountain building started in the Oligocene (Chedia 1980) or even later (Abdrakhmatov et
 108 al. 1996), forming a complex system of basement folds disrupted by numerous thrusts and reverse faults with
 109 significant amount of lateral offset (Delvaux et al. 2001). Several regional fault zones are aligned along large parts
 110 of the mountain belts, others cross the orogen in a NW-SE direction, e.g., the Talas-Fergana fault, which forms a
 111 distinct boundary between the western and central Tien Shan (Trifonov et al. 1992) (Fig. 2).



112
 113 **Figure 1. Study area geographical-geomorphological setting.** Lakes' polygons from Schiavina et al., 2022,
 114 while MERIT DEM (Yamazaki et al. 2017) was used as topographic base.

115 Mountain ridges, formed mainly by palaeozoic crystalline rocks, are separated by wide lenticular or narrow, linear
 116 intermountain depressions, containing Neogene and Quaternary deposits, mainly sandstone, siltstone with gypsum
 117 interbeds, and conglomerates (Strom and Abdrakhmatov, 2017). Mesozoic and Paleogene deposits are typical of
 118 the foothill areas. Almost every ridge, especially in the Tien Shan, corresponds to a neotectonic anticline, and most
 119 of the main river valleys follow intermontane tectonic depressions, which are linked by narrow deep gorges up to
 120 1-2 km deep (Strom and Abdrakhmatov, 2018). These mountain systems are the sources of most of Central Asia
 121 rivers, which, being fed by glaciers, snowmelt water and rain, have deeply incised valleys. Such extreme
 122 topography along with complex geological structure, active tectonics and high seismicity determine important

123 landslide predisposing factors, making landslides the third most prevalent natural hazard in Central Asia, following
 124 earthquakes and floods (CAC DRMI, 2009; Havenit et al, 2017).



125
 126 **Figure 2. Geological map of the study area.** Geological formation data from United States Geological Survey
 127 (see Persits et al., 1997 for the legend), including faults from the AFEAD (Active Faults of Eurasia) database
 128 (Styron and Pagani, 2020).

129 **2.1 Landslide types in Central Asia**

130 According to the international Cruden and Varnes 1996 classification, landslides phenomena in Central Asia
 131 include rockslides/rock avalanches, rotational/translational slides and mud/debris flows (often involving loess),
 132 which are triggered by natural events such as earthquakes, floods, rainfall and snowmelt (Behling et al., 2014;
 133 2016; Golovko, 2015; Havenith et al., 2006a,b, 2015a, b; Kalmetieva et al., 2009; Saponaro et al., 2014; 2015;
 134 Strom and Abdrakhmatov, 2017; 2018). Glacial lakes outburst flood phenomena, caused by the breach of natural
 135 glacial dams, often result in large scale catastrophic mud/debris flows. In Central Asia, landslides more often occur
 136 in the loess zone of contact with other rocks, on clay interlayers of the Mesozoic and Cenozoic age, reaching a
 137 volume from tens of thousands up to $15-40 \cdot 10^6 \text{ m}^3$ (Juliev et al., 2017). Seismically triggered landslides are very
 138 common in tectonically active mountain regions, such as Tien Shan and Pamir (Sternberg et al., 2006; Hong et al.,
 139 2007; Juliev et al., 2017). According to the literature background, most of the large mapped mass movements
 140 (especially those with a volume of more than 10^6 m^3) were triggered generally by major (also prehistoric)
 141 earthquakes, possibly in combination with climatic factors, namely snowmelt and heavy rainfall (Havenith et al.,
 142 2003; Strom and Korup, 2006; Strom, 2010; Schlögel et al., 2011; Strom and Abdrakhmatov 2017, 2018; Havenith
 143 et al., 2015a; 2016; Behling et al., 2014; 2016; Piroton et al., 2020). Furthermore, in the past few decades, the
 144 number and intensity of landslides have grown owing to climate change and the increase of the anthropic pressure,
 145 due to several factors such as the uncontrolled land and water use, the rising of the water tables (often induced by

146 the increase of Irrigation; Ishihara et al., 1990), mining, and excavation activities (Pollner et al., 2010; Thurman,
147 2011).

148 **2.2 Large Rockslides and natural dams**

149 Numerous rockslides have occurred in the mountains producing hazardous natural phenomena such as long runout
150 rock avalanches (Fig. 3) and dammed lakes, more than 100 of which still store water (Strom, 2010). These mainly
151 involve the Palaeozoic magmatic and metamorphic crystalline bedrock, but also the sandstone and limestone
152 formations. Although according to Strom, 2010, many of the existing dammed lakes should be considered as stable,
153 catastrophic outburst floods that occurred in the 20th century, emphasize high potential hazard of landslide natural
154 blockages. Havenith et al., 2015a report a catalogue of large to giant landslides (having volumes exceeding $>10^7$
155 m^3) in the Tien Shan area, showing several information such as location, time of occurrence, volumes, and
156 thickness. Regarding the volumes of these rockslides, these range from $50 \cdot 10^3 m^3$ to $10 km^3$ (Strom and Korup,
157 2006; Strom and Abdrakhmatov, 2018). Many of these phenomena, though not all, were triggered by earthquakes
158 with $M > 6$ and have dammed a river valley (some of the dams have been naturally or artificially breached).

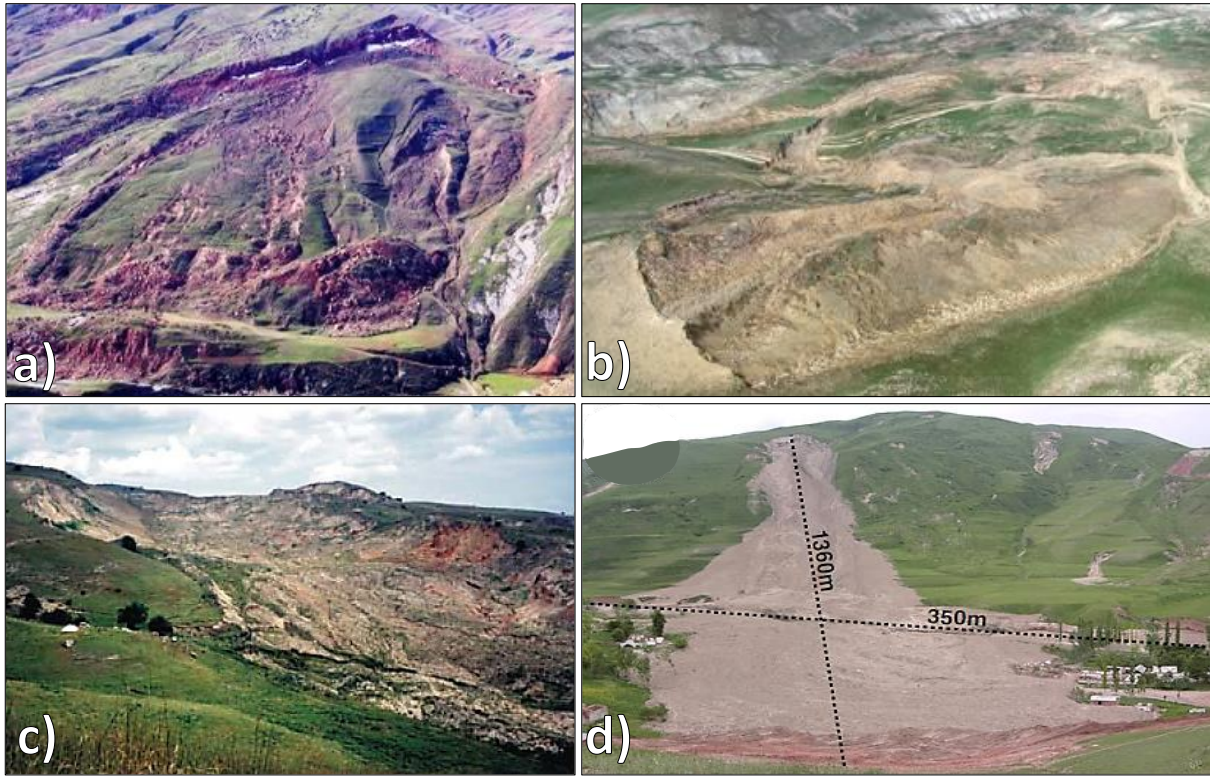


159
160 **Figure 3. Examples of large rockslide features in Central Asia.** Helicopter view of the Usoi landslide scarp,
161 triggered by the 1911 earthquake, Tajikistan (a) (after Strom, 2010); Khait rock avalanche (b) (after Havenith et
162 al., 2015a); helicopter view of Ananevo landslides (c) (after Havenith et al., 2015a).

163 **2.3. Landslide in soft rocks and loose deposits**

164 Rotational landslides mostly occur in loose unconsolidated Quaternary deposits, and in soft and semi-hard rock
165 layers in Mesozoic-Cenozoic sediments, represented mainly by layers of clays, claystones, siltstones, sandstones,
166 marls, limestone, gypsum, and conglomerates, with intercalated clays (Roessner et al., 2004; Kalmetieva et al.,
167 2009) (Fig. 4). These phenomena can create river dams, but they rarely are long-living dams, since usually they
168 are small and their bodies are eroded quickly even if they block a river channel (Strom and Korup, 2006).

169 The loess landslides occur quite regularly (on a yearly basis) in the regions presenting an almost continuous and
170 locally very thick (>20 m) cover of this material, generally at mid-mountain altitude (900– 2,300 m) and mainly
171 along the border of the Fergana Basin (Kyrgyz Republic, Uzbekistan, and Tajikistan), and on the southern border
172 of the Tien Shan in Tajikistan (Fig. 4).



173
174 **Figure 4. Examples of landslides in soft rocks-loose deposits.** Picture the Kamar landslide (a) and the Beshbulak
175 landslide (b) (after Niyazov and Nurtaev, 2013). Examples of loess slides and mixed loess—soft landslides in NE
176 Fergana valley: Kochkor-Ata landslide failure in spring 1994 (c) (after Roessner et al., 2005); Field photo of the
177 Kainama landslide (d) (after Behling et al., 2016).

178 Loess flow landslides and debris flows, involving the eluvial slope cover, represent a relevant hazardous
179 phenomenon in the mountainous regions of Kazakhstan, in the area of Almaty, near the southern border with
180 Kyrgyz Republic, in the Altai area (Medeu and Blagovechshenskiy, 2016), around the Fergana Basin, all along
181 the border between Tajikistan and Kyrgyz Republic and around the Tajik Depression. Landslides occurring in
182 Quaternary loess units of up to 50 meters thick are characterized by very rapid avalanche-like mass movements,
183 which can reach several meters per second (often represent a combination of rotational slide and dry flow resulting
184 in long runout zones; World Bank, 2008). Typically, pure loess landslides have a volume of hundreds up to one
185 million cubic meters and appear as clusters (Roessner et al., 2005). From the recent history it appears that pure (or
186 quasi-pure) loess slides and flows are particularly dangerous because of their high velocity and long runout which,
187 in turn, can generate a great destructive power and more severe disasters than other types of mass movements of
188 similar size (Havenith et al., 2015a; Behling et al., 2014; 2016). If failure also affects underlying materials (mostly
189 Mesozoic and Cenozoic soft rocks), the volume of these mixed slides can exceed $10 \times 10^6 \text{ m}^3$.

190 These kinds of landslides are particularly deadly and can be triggered by a combination of long-term slope
191 destabilization factors (e.g., rainfall and snowmelt) and short-term triggers (e.g., seismic shocks). Even though
192 earthquake-triggered loess slides and flows are far less frequent than rainfall triggered ones, they caused much
193 larger disasters in recent history, such as those triggered, respectively, by the July 1949 Khait and the January 1989
194 Gissar earthquakes. The number of active debris flow basins in Kazakhstan is over 300 with registered cases of
195 more than 600 debris flows of different genesis (80% of which are represented by heavy rainfall-triggered debris
196 flows, while the glacial debris flows make up about 15% of the total) (Yaning, C., 1992).

197 **3 Materials and Methods**

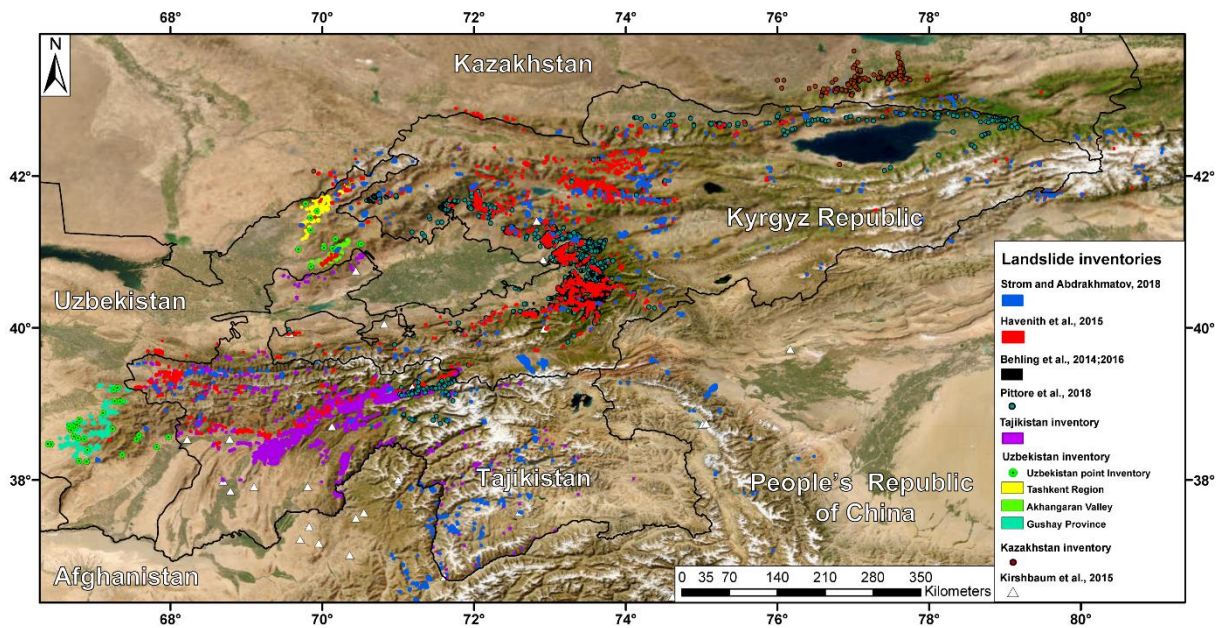
198 **3.1 Landslide databases**

199 To implement the adopted susceptibility models the largest, most accurate, and updated landslide inventories were
200 used (Fig. 5). These were compiled by several authors by means of decades of field surveys, remote sensing and
201 geophysical analysis in the study area.

202 Hereafter we report their description in detail (Tab. 2):

- 203 • The “Tien Shan landslide inventory” (Havenith et al., 2015a): represents the largest inventory in the study
204 area. Compiled by means of field surveys, remote sensing data interpretation and geophysical surveys, it
205 comprises the rockslides of the previous inventory together with other smaller landslides in soft sediments
206 (Havenith et al. 2006a; Schlögel et al., 2011) for a total of 3,462 landslides polygons, also including
207 information on landslide length and area.
- 208 • The “Rockslides and Rock Avalanches of Central Asia” (Strom and Abdrakhmatov, 2018): a large inventory
209 including 860 polygons of large-scale ($\geq 1 \text{ Mm}^3$) rockslides and rock avalanches, covering central Asian
210 countries (except for Turkmenistan and Altai) plus Chinese Tien Shan and Pamir, and Afghan Badakhshan.
211 Compiled in decades of field work and analysis of aerial/satellite imaging, it also comprises information on
212 landslide morphometric parameters (runout, area), and 126 polygons on possible landslide bodies, dammed
213 lakes, and head-scarps. Quantitative characteristics (area, volume, runout, etc.) for about 600 cases are
214 provided as well.
- 215 • The “Multi-temporal landslide inventory for a study area in Southern Kyrgyz Republic derived from RapidEye
216 satellite time series data (2009 – 2013)” (Behling et al., 2014; 2016; 2020), is a semi-automated spatiotemporal
217 landslide inventory for the period from 1986 to 2013, covering a 2,500 km² in the Fergana valley rim in
218 southern Kyrgyz Republic. This inventory includes 2,052 landslide polygons mapped from multi-sensor
219 optical satellite time series data, together with information on spatiotemporal landslide activity patterns (area
220 and year of trigger).
- 221 • “The EMCA landslide catalogue Central Asia” (Pittore et al., 2018), including 3,129 points, which covers
222 mostly western and northern Kyrgyz Republic as well as Tajikista’s Region of Republican Subordination.
223 The catalogue is a summary (point locations) of the documented landslides between 1954 and 2009
224 (Kalmatieva et al., 2009), which are collected by the Central Asian Institute for Applied Geosciences through
225 geological surveys (field campaigns) on single sites close to urban areas.

- The “Tajikistan landslide database” provided by the Institute of Water problems, Hydropower, Engineering and Ecology of Tajikistan (IWPHE), which includes 2,822 landslide polygons and 114 landslide-prone areas (with information on length and area).
- The “Uzbekistan landslide inventory” provided by the Institute of Seismology of the Academy of Science of Uzbekistan (ISASUZ) and the State Monitoring Service of the Republic of Uzbekistan for hazardous geological processes, which covers the Tashkent-Gushay provinces, and the Akhangan Valley. It comprises a 49-point inventory (including location, type, volume, length, and date of triggering; Nyazov R.A. 2020) and a polygon inventory digitized for this project from the maps in Juliev et al., 2017 (including a total 324 landslide polygons).
- The “Kazakhstan landslide inventory”, provided by the Institute of Seismology Limited Liability Partnership (LLP) of Kazakhstan, covering mainly the Tien Shan area at the border with Kyrgyz Republic, and small part of the western Altai, including 254 point-objects with information on type, area/volume, triggering date.
- Part of the “Global Landslide Catalogue (GLC)” (Kirshbaum et al., 2015), which covers Kyrgyz Republic and Tajikistan, including 15 landslide point with a description on landslide size/type and triggering date/factor. The GLC was compiled since 2007 at NASA Goddard Space Flight Centre NASA and considers all types of mass movements triggered by rainfall, which have been reported in the media, disaster databases, scientific reports, or other sources.



243
244 **Figure 5. Map of the adopted landslide inventory.** Basemap source: Esri, Maxar, Earthstar Geographics, and
245 the GIS User Community.

246
247
248
249

Table 2. Name of the Landslide Inventory Maps (LIM) of the study area.

LIM name	Author	Covered country	Type of element	N° of elements	Web reference
Tien Shan landslide inventory	Havenith et al., 2015a	Kazakhstan, Kyrgyz Republic, Tajikistan, Uzbekistan, People's Republic of China	Polygons	3,462	https://www.sciencedirect.com/science/article/abs/pii/S0169555X15000665?via%3Dihub
Rockslides and Rock Avalanches of Central Asia	Strom and Abdrakhmatov, 2018	Kazakhstan, Kyrgyz Republic, Tajikistan, Uzbekistan, Afghanistan, People's Republic of China	Polygons	986	https://www.sciencedirect.com/book/9780128032046/rockslides-and-rock-avalanches-of-central-asia
Multi-temporal landslide inventory for a study area in Southern Kyrgyz Republic derived from RapidEye satellite time series data (2009 – 2013)	Behling et al., 2014; 2016; 2020	Kyrgyz Republic	Polygons	2,052	https://dataservices.gfz-potsdam.de/panmetaworks/showshort.php?id=escidoc:5085890
The EMCA landslide catalogue Central Asia	Pittore et al., 2018	Kyrgyz Republic, Tajikistan	Points	3,129	https://dataservices.gfz-potsdam.de/panmetaworks/showshort.php?id=escidoc:3657915
Tajikistan landslide database	Institute of Water problems, Hydropower, Engineering and Ecology	Tajikistan	Polygons	2,822	N.A.

	of Tajikistan (IWPHE)				
Uzbekistan landslide inventory	Institute of Seismology of the Academy of Science of Uzbekistan (ISASUZ), State Monitoring Service of the Republic of Uzbekistan for hazardous geological processes, Nyazov R.A. 2020, Juliev et al., 2017	Uzbekistan	Polygons/ Points	375	N.A.
Kazakhstan landslide inventory	Institute of Seismology Limited Liability Partnership (LLP)	Kazakhstan, Kyrgyz Republic	Points	254	N.A.
Global Landslide Catalogue (GLC)	Kirshbaum et al., 2015	Kyrgyz Republic, Tajikistan, Uzbekistan	Points	15	https://svs.gsfc.nasa.gov/4710

251 **3.2 Random Forest (RF) model**

252 To generate the landslide susceptibility maps in this work, the Random Forest model (RF) was used. The RF is a
253 nonparametric and multivariate machine learning technique, which was proposed by Breiman (2001), and first
254 used in landslide susceptibility analysis by Brenning (2005). Since then, it has rapidly gained widespread
255 consolidation through many research and case studies, as it is considered a relatively powerful approach in
256 classification, regression, and unsupervised learning (Lagomarsino et al., 2017). Among the advantages of using
257 the RF algorithm, there is the possibility of using numerical and categorical variables at the same time, without
258 assumption on the statistical distribution of their values. Furthermore, RF is acknowledged to be capable of
259 handling implicitly the multicollinearity of variables, identifying the uninfluential (or the detrimental) ones

260 (Breiman, 2001; Brenning, 2005). The RF also automatically performs a validation by building a Receiver
261 Operating Characteristic Curve (ROC Curve) and calculates the relative Area Under the Curve (AUC). AUC is
262 widely used as a quantitative indicator for the predictive effectiveness of susceptibility models: it can range from
263 0.5 (completely random predictions) to 1.0. This model, by means of the bootstrapping technique, also calculates
264 the Out-of-Bag Error (OOBE) for each variable. This parameter measures the relative error that would be
265 committed if a given variable is excluded from the RF classifier. OOBE can be used to assess the relative
266 importance of each independent variable, thus representing a powerful tool to interpret the results and to rank the
267 variables according to their importance (Catani et al., 2013). RF contains a series of binary tree predictors, which
268 are generated by using a random selection of the input data (the independent variables which in LSM studies, are
269 a set of physical parameters representing the predisposing factors), in order to split each binary node (yes/no), and
270 to perform a classification of the target dependent variable (in LSM studies, the presence or absence of landslides).
271 Some of the observations are used for internal testing to evaluate the predictive capability of each predictor tree.
272 This information is used to iterate the procedure hundreds of times by growing other random trees (hence the name
273 “Random Forest”), and to iteratively adjust the prediction effectiveness. Once the best predictor tree is identified,
274 it is applied to the whole study area, to define the LSM. Another important key point of RF is that it has a great
275 predictive performance and runs fast by summarizing many classification trees and this is particularly useful when
276 dealing with large amounts of data.

277 **3.3. Selection of independent variables**

278 As independent variables, twenty “basic parameters” were selected in all 5 countries, based on the available data
279 and according to the ones most widely adopted in literature (Catani et al., 2013; Reichenbach et al., 2018). Many
280 of these are DEM-derived products (e.g., elevation, aspect, slope, slope curvature, flow accumulation, Stream
281 Power Index, Topographic Wetness Index, Topographic Position Index). It must be considered that the resolution
282 of the susceptibility maps depends on the resolution of the input data. Therefore, it was decided to use pixels
283 corresponding to the MERIT DEM (Yamazaki et al. 2017) resolution (“about 90 m at equator and 70 m at 40°
284 latitude). In addition, the DEM itself was used as a reference map, so that the other parameters were processed to
285 have a perfect overlapping. Therefore, the resulting landslide susceptibility maps will also be perfectly overlapping
286 to it. The variables such as lithology and soil type were rasterized with this resolution by choosing the most
287 frequent value in a reference window. The twenty “basic parameters” used are listed below, including a brief
288 description:

- 289 • MERIT DEM and DEM-derived products: Aspect, Slope Gradient, Total Curvature, Profile Curvature, Planar
290 Curvature, Flow Accumulation, Topographic Wetness Index (TWI), Stream Power Index (SPI), Topographic
291 Position Index (TPI).
- 292 • Lithology, derived from the geological map of the former Soviet Union made by the USGS (Persits et al. 1997).
- 293 • Soil type map from the DSMW database (Copernicus land use; <https://land.copernicus.eu/>).
- 294 • Distance from Faults: it is minimum distance, in meters, between each landslide and the nearest fault. The fault
295 database is derived from the AFEAD catalogue (Styron and Pagani, 2020) and was modified after Poggi et al.,
296 a (in prep.).

- Distance from Roads: it is minimum distance, in meters, between each landslide and the nearest road. The roads database is derived from Scaini et al., (in prep.).
- Distance from Rivers: it is minimum distance, in meters, between each landslide and the nearest river. The river network database is derived from Coccia et al., (in prep.).
- Distance from Hypocentres: it is minimum distance, in meters, between each landslide and the nearest earthquake hypocentre with a magnitude greater than 6.5 (following the methodology adopted by Havenith et al., 2015a). The Hypocentre database was provided by Poggi et al., a (in prep.).
- Peak Ground Acceleration (PGA): 4 kind of PGA maps according to different return times (475 and 1000 years) and different materials (soil layers and bedrock) to which it refers were created (Poggi et al. b, in prep.).

In addition to these “basic parameters”, in this study it was decided to use five parameters related to the propensity of the territory to be affected by precipitation (Fig. 6). These parameters were obtained from the ERA5 database (www.ecmwf.int/en/forecasts/datasets/reanalysis-datasets/era5).

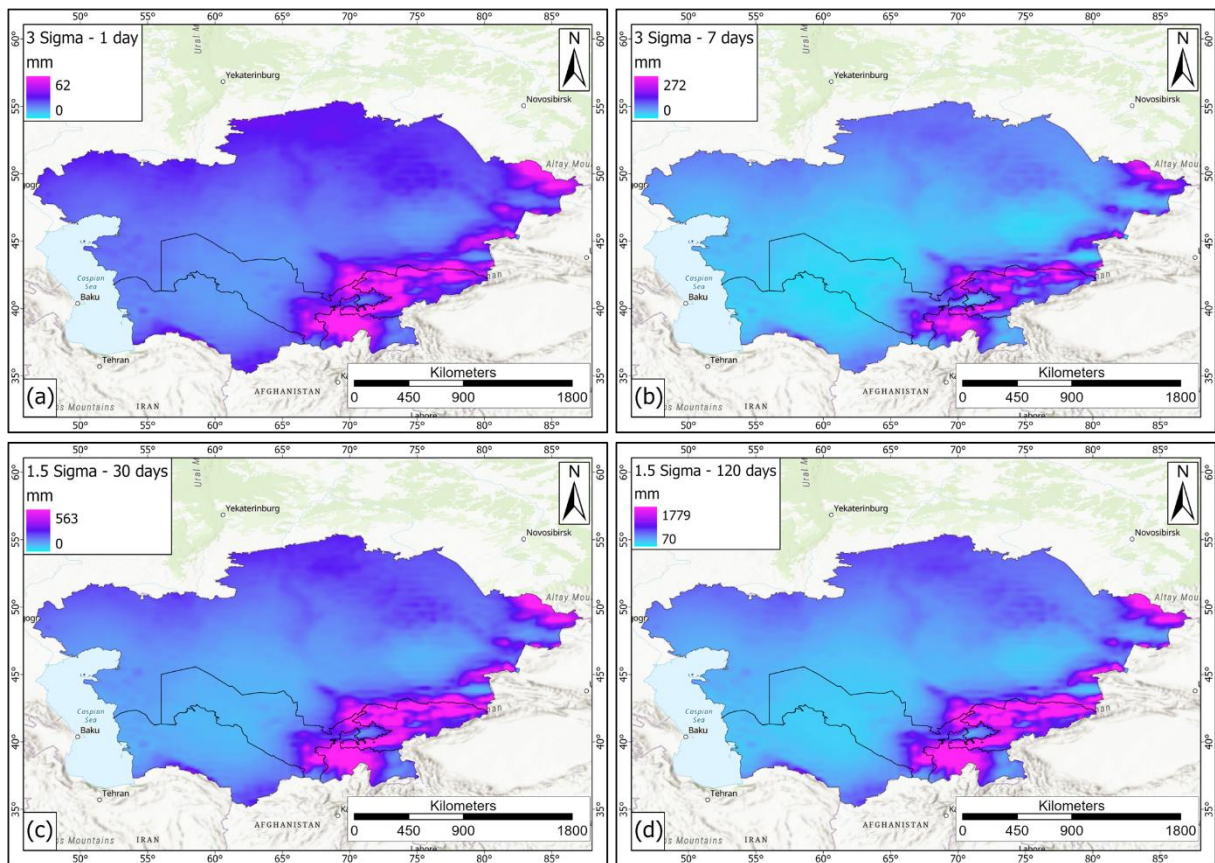


Figure 6. Rainfall maps from the ERA5 database (www.ecmwf.int/en/forecasts/datasets/reanalysis-datasets/era5). (a) rainfall amounts corresponding to 3 standard deviations for 1-day rainfall; (b) rainfall amounts corresponding to 3 standard deviations for 7-days rainfall; (c) rainfall amounts corresponding to 1.5 standard deviations for 30-days rainfall; (d) rainfall amounts corresponding to 1.5 standard deviations for 120-days rainfall. Basemap source: Esri, USGS, NOAA.

315 Rainfall distribution maps have been used to differentiate the study area based on the rain rate and the distribution
316 of anomalous rainfall events, since more rainy areas are more likely to experiment landslide events than those less
317 rainy. At the same time, a rain event with a low probability of occurrence can likely trigger a landslide even in less
318 rainy areas, so the probability of some extreme rainfall events was calculated as well. These data span from 1981
319 to 2020, have a 1-hour temporal resolution (summarized to daily resolution for this work) and a spatial resolution
320 0.25° . The first parameter is the Mean Annual Precipitation (MAP) map, where, for each pixel, the mean annual
321 precipitation was calculated (Fig. 6). Other maps (named Sigma maps) have been calculated by the spatialization
322 of the approach described in Martelloni et al (2011). In detail, for each rain gauge (represented by the pixels of
323 ERA5 maps in this work) the rain values corresponding to a given standard deviation for several cumulative
324 intervals are defined (e.g., the rain values corresponding to 2 standard deviations of the distribution of 3-days
325 cumulative rainfall):

- 326 • Sigma 1.5 – 120 days: rainfall values corresponding to 1.5 standard deviations of the 120-days cumulative
327 rainfall. They range from 70 mm to 1778.8 mm (Fig. 6a).
- 328 • Sigma 1.5– 30 days: rainfall values corresponding to 1.5 standard deviations of the 30-days cumulative rainfall.
329 They range from 0 mm to 563.1 mm (Fig. 6b).
- 330 • Sigma 3– 1 days: rainfall values corresponding to 3 standard deviations of daily cumulative rainfall. They
331 range from 0 mm to 62.2 mm (Fig. 6c).
- 332 • Sigma 3– 7 days: rainfall values corresponding to 3 standard deviations of the 3-days cumulative rainfall. They
333 range from 0 mm to 271.9 mm (Fig. 6d).

334 The sigma parameters represent the probability of having a given rainfall amount over a defined time interval. In
335 this work, four intervals were selected (1, 7, 30 and 120 days) to consider both short and long rain events, that can
336 lead to the triggering of surficial or deep-seated landslides, respectively. For 1 and 7 days the maps of the rainfall
337 values corresponding to 3 standard deviations over the mean rainfall were selected, to verify if short and very
338 intense rainfall (with a very low probability of occurrence) could influence the slope stability in the study area.
339 Regarding the 30-days and 120-days interval, rainfall values corresponding to 1.5 standard deviation were
340 calculated, in order to assess the influence of longer and less intense rainfalls over slope stability.

341 **3.4. Model optimization**

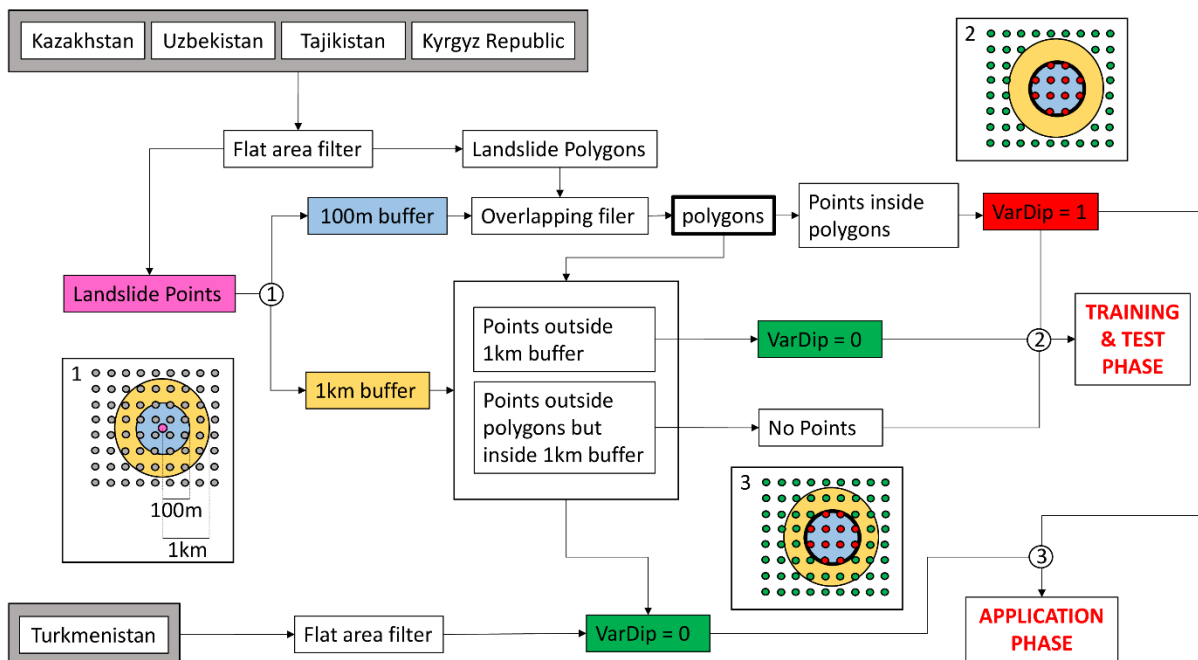
342 *3.4.1 Independent variables optimization*

343 The LSM was defined using the whole study area, instead of processing each country individually. This choice
344 allowed to overcome the boundary effects associated with the use of independent countries. In addition, a buffer
345 of 10 km was considered around the whole area, to avoid deformation due to boundary effects. These choices were
346 helpful in reducing distortions and improving the quality of the results, but also led to a huge amount of data to be
347 processed. Since the same resolution of the DEM was used for susceptibility assessment, the whole area was
348 divided into about $1.07 * 10^9$ cells and for each cell 26 condition factors and 1 dependent variable were defined;
349 this led to about $2.89 * 10^{10}$ data to be processed. In order to reduce the processing time and avoid computational
350 problems due to the huge amount of data and to the width of the study area, large flat areas were filtered and not
351 considered in the modelling process, since landslides generally take place along slopes (some exceptions to this

352 statement in the area are represented by landslide around the flat Caspian Sea area (Pánek et al., 2016)). For
 353 Turkmenistan no landslide database was available, so it was decided to train and test the model only with the other
 354 4 countries, to obtain the best predictor model for the available data. The trained model has then been applied to
 355 the whole study area, including Turkmenistan, to define the LSM.

356 3.4.2 Landslide Inventory Harmonization

357 Regarding the dependent variables, the landslides inventory was created by merging the data described in section
 358 3.1. As a result, this landslide dataset was quite heterogenous, hence an initial control and homogenization phase
 359 was necessary. In this framework the landslide data were checked to verify the presence of overlapping polygons
 360 or topological errors, which were removed. Since some landslide inventories were composed solely by points,
 361 these were mapped only as a “landslide points”, a 100 m buffer was created around them, in order to include them
 362 in the model. However, when the points refer to large landslides, which are frequent in the study area, it is possible
 363 that part of the body of these landslides is still outside the perimeter achieved with the buffer. To avoid classifying
 364 these areas as non-landslide points, it was decided to create an additional buffer of 1 km around points, used as a
 365 mask where the non-landslide points were not to be selected. This process reduced the probability of pixels
 366 misclassification (e.g., landslide points considered as non-landslide points) during the training of the model. All
 367 the points inside the 1-km buffer were only considered during the model application, as well as point from
 368 Turkmenistan. Some landslide-prone areas were also present in the input inventories; since these were not real
 369 landslides but ‘landslide-prone zones’, these areas were not used to train the susceptibility model but were used in
 370 the validation of the results. This optimization procedure, schematized in Fig. 7, allowed to define an input dataset
 371 of $1.08 \cdot 10^8$ points (along with 27 variables for each point) to be used to define the susceptibility model.

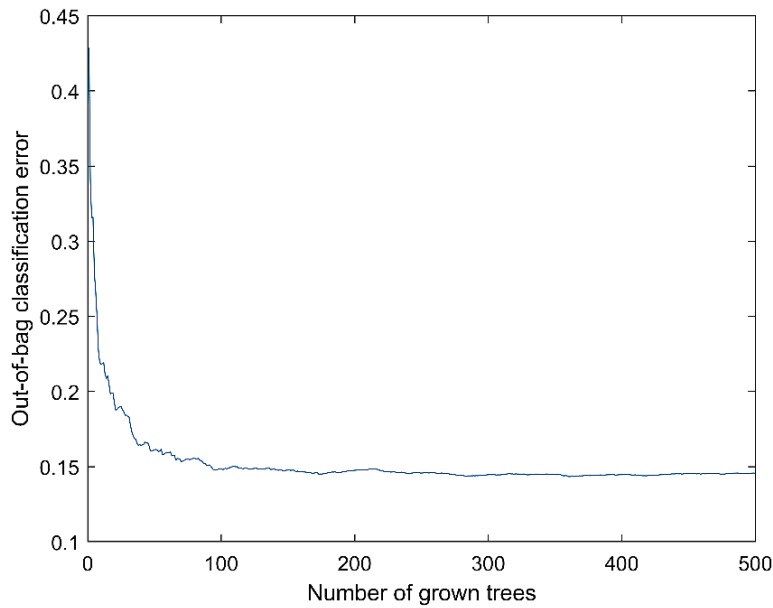


372

373 **Figure 7. Workflow describing the landslides database harmonization procedure.** In gray: sample points for
 374 RF; pink: landslide points; blue: 100m buffer; yellow: 1km buffer; red: sample points identified as vardip=1; green:
 375 sample points identified as vardip=0; bold black line: landslide body; VarDip=dependent variable.

376 **3.4.3 Trees number optimization**

377 A further optimization of the model was performed by the evaluation of the out of bag classification error, i.e., the
378 variation of the misclassification probability with the number of grown classification trees. The classification error
379 initially reduces with the increasing of classification trees, then it turns to be stable, so the definition of the optimal
380 number of classification trees is required to avoid the use of an overgrown forest with an excessive number of trees
381 (hence with high computational load and time) and without any advantage for the model (Fig. 8).



382

383 **Figure 8. Example of out of bag classification error.** The error is stable using 100 or more trees.

384 **3.5. Model training**

385 Once all the data were prepared and organized, the algorithm to create the landslide susceptibility maps was
386 developed. A crucial step in LSM analysis is the approach used to sample the variables to train and validate the
387 model. As in any other statistical procedures, the size of the dataset influences the results, therefore the higher the
388 number of samples to perform the statistical calibration/validation of the model, the more reliable are the obtained
389 results. To avoid a generalized hazard overestimation, Catani et al. (2013) demonstrated that a random sampling
390 improves the predictive capability of the map, and that the susceptibility model should also be trained/validated
391 with respect to information about non-landslide locations. Regarding the proportion between the calibration and
392 validation dataset samples, it is common practice to split them according to a 70/30 ratio. Therefore, using ESRI
393 ArcGIS Pro software, all the variables were sampled pixel by pixel, after which, with the Matlab software, from
394 the total of the sampled points, all the points within a landslide and a same amount of randomly chosen non-
395 landslide points were extracted. This input dataset was divided into two parts, 70% of the data (calibration dataset)
396 was used for the training phase, and the remaining 30% (validation dataset) for the testing phase. The selection
397 and division were randomly repeated 5 times, in order to assess the stability of the model to the variation of the
398 training and testing datasets, hence, to verify the absence of overfitting issues. Each one of these datasets was
399 created to be equally composed by pixel within a known landslide and pixel outside a landslide.

400 All these data were then used to train and test the algorithm created to predict the landslide susceptibility of the
401 whole area. The best predictor model identified in the training phases was then applied to all the available data
402 (also for Turkmenistan and for the 1-km buffer area around the point-object landslides) for the development of the
403 susceptibility map on the whole Central Asia area. The results obtained from the application of the aforementioned
404 methodology are the susceptibility map, the ROC (Receiver Operating Characteristic) curves with their AUC (Area
405 Under the Curve) values, and the histogram of the importance of variables. ROC and AUC are used to verify the
406 quality of the landslide susceptibility model, both by graphical and analytical approach. Due to the high volume
407 of data, their variety, values, and heterogeneity a specific algorithm was created for this work, that was set to be
408 able to perform several activities:

- 409 • Reading and properly formatting the input data and then dividing them between independent and
410 dependent variables.
- 411 • Automatically and randomly selecting locations associated with landslides or outside landslides to create
412 the training and test datasets.
- 413 • Identifying the best predictor and evaluating its performances by the calculation of the misclassification
414 probability of the values calculated by the model.
- 415 • Evaluating the overall performances of the model by the mean of ROC and AUC.
- 416 • Identifying the importance of the parameters in landslide susceptibility.
- 417 • Applying the model to the whole study area, calculate the probability of classification (landslide or non-
418 landslide) of each pixel and extraction of the final map in raster format.

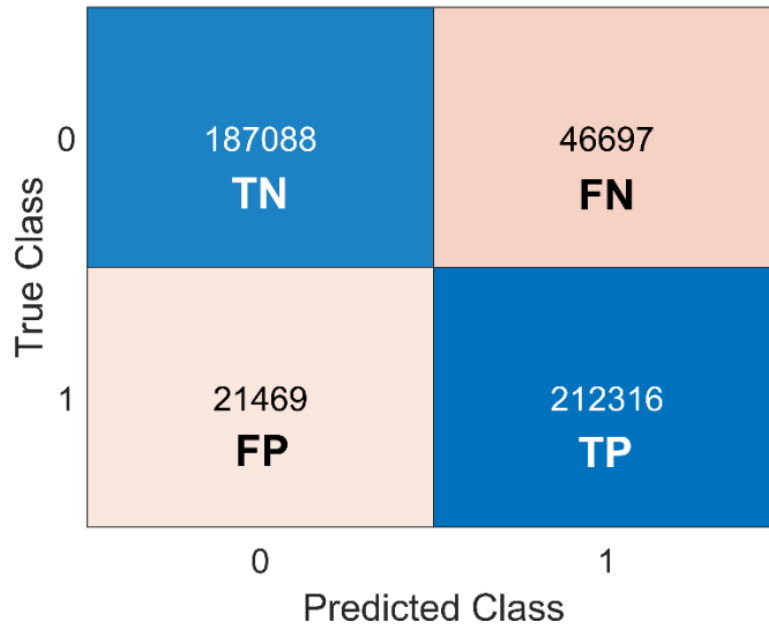
419 The algorithm was set to work in classification mode, e.g., for each pixel a value (1 or 0) is assigned to identify
420 the presence or absence of a landslides (dependent variable), along with the values of the independent variables.
421 Using these data, the RF model identifies the best association of independent variables linked to presence or
422 absence of landslides (landslide susceptibility prediction model). The prediction model is then applied to all the
423 pixels of the investigated area, and the probability of each pixel to be classified as landslide (or non-landslide)
424 pixel is evaluated. These probability values are those used to create the landslide susceptibility maps. It must be
425 noticed that the landslide inventories adopted to train the RF rarely reported the type of landslide, so the LSMs
426 must be considered not related to a specific type of landslide.

427 **3.6. Model validation**

428 To verify the quality of the susceptibility models, beside the AUC value previously reported, a confusion matrix
429 for the four countries where the model was trained was created (Fig. 9). In each matrix the predicted landslide
430 classes are compared with the ground truth to verify the presence of significant misclassification error. In all the
431 matrix the value 1 represent the presence of landslide, the value 0 represents the absence of landslides; the numbers
432 in each cell represent the number of pixels classified in that combination of 0 and 1, according to this scheme (the
433 first number represent the predicted class, the second number the ground truth):

- 434 • 0-0 (True negative): pixels outside any landslides are correctly identified as no-landslide pixels by the
435 model.
- 436 • 1-1 (True positive): pixels inside a landslide are correctly identified as landslide pixels by the model.

- 437 • 0-1 (False negative): pixels inside a landslide are wrongly identified as no-landslide pixels by the model.
- 438 • 1-0 (False positive): pixels outside any landslides are wrongly identified as landslide pixels by the model.



439

440

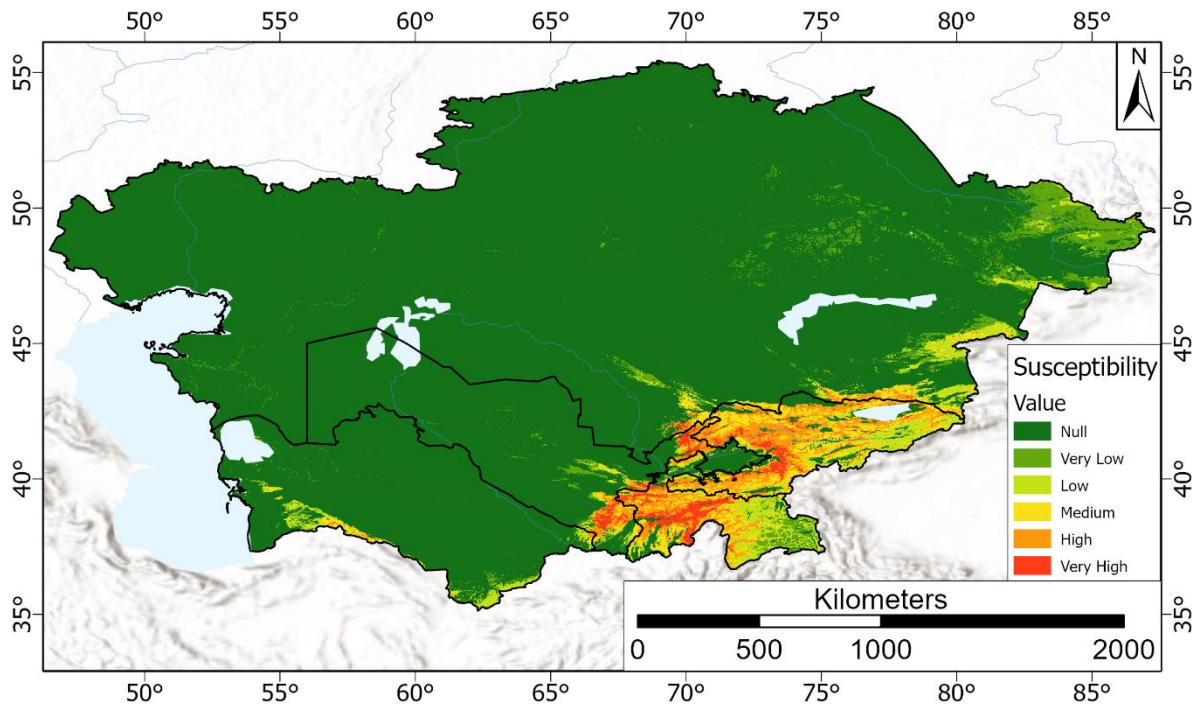
Figure 9. Confusion matrix for the four countries where the model was trained.

441 The 0-0 and 1-1 combinations represent well classified pixels (blue cells in Fig. 8), while 0-1 and 1-0 represent
 442 misclassification error (light red cells in Fig. 8). Since this matrix needs some ground-truth parameters (True
 443 classes), it can be applied only where the presence or absence of landslides is known. For this reason, in this work,
 444 this matrix was calculated considering only the test dataset. A further control of the results was made using the
 445 areas prone to landslides identified in the used landslide inventories.

446 **4. Results**

447 **4.1 Susceptibility map**

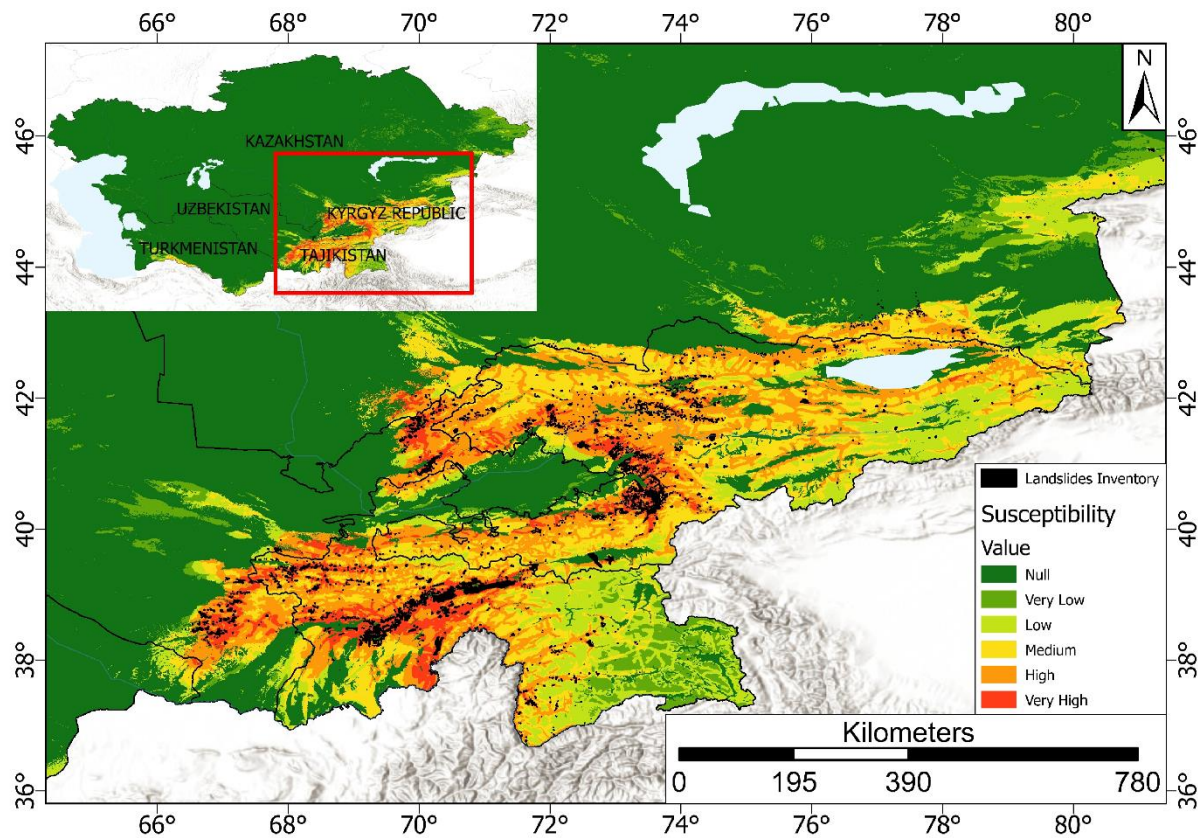
448 In the map presented in the following Figures 10 and 11, the susceptibility values, ranging from 0 to 1, were
 449 classified into five classes (Table). Here the corresponding extension and percentage of the study area are also
 450 reported, showing that the most frequent susceptibility class for the whole study area is the null class (=87.8%;
 451 landslides generally don't occur in flat areas), followed by low and medium classes. Only the 4% of the central
 452 Asian territory is represented by areas with high and very high landslide susceptibility (Table). In Fig. 12, the
 453 susceptibility maps of five selected areas are displayed to better show the details of the susceptibility assessment,
 454 and its comparison with mapped landslides in different geomorphological contexts of the study area. From these
 455 details it is possible to ascertain the high usefulness of the landslide susceptibility map realized by applying the
 456 Random Forest model, which, mainly based on the hydro-geomorphological properties, can establish the degree
 457 of susceptibility even in areas where there is no awareness of the predisposition to instability due to the absence
 458 of reported landslides.



459

460

Figure 10. Landslide susceptibility map of Central Asia. Basemap source: Esri, USGS, NOAA.



461

462

463

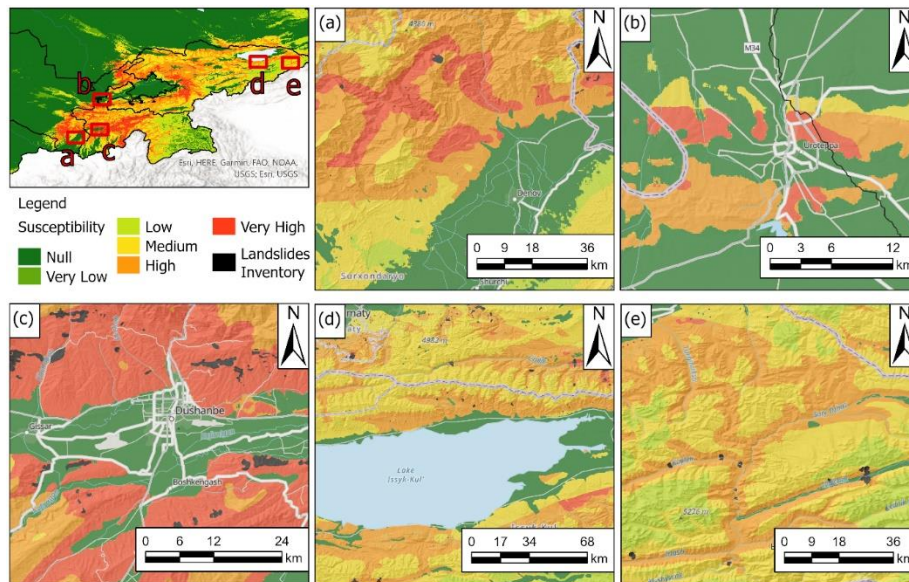
Figure 11. Detail of the landslide susceptibility map with the overlapping landslide polygons (in black). On the top left the detailed area with respect to the central Asian territory. Basemap source: Esri, USGS, NOAA.

464 **Table 3.** Landslide susceptibility class intervals, corresponding area, and percentage with respect to CA.

Susceptibility class	Landslide spatial probability interval	Corresponding area (km ²)	Corresponding percentage of CA (%)
Null	0 - 0.05	2,889,481.2	87.8
Very Low	0.05 - 0.25	94,674.7	2.9
Low	0.25 - 0.35	85,294.1	2.6
Medium	0.35 - 0.45	87,528.5	2.7
High	0.45 - 0.6	99,689.8	3
Very High	0.6 - 1	31,436.4	1

465 In particular:

- 466 • Fig. 12a shows the area north of the city of Denau, in the south-east of Uzbekistan, which is characterized
 467 by a high susceptibility, despite the almost total absence of mapped landslides.
- 468 • Fig.12b shows a detail of the city of Ura-Tube, in the North-West of Tajikistan, where there are not any
 469 known landslides, but a high susceptibility has been obtained in the surrounding mountain relief.
- 470 • In Fig. 12c there is a close-up on the city of Dushanbe, the capital of Tajikistan, where close to roads and
 471 inhabited centres a high landslides susceptibility is observed.
- 472 • The shores of Lake Issyk-Kul in the Kyrgyz Republic, shown in Fig. 12d, are generally flat areas, with a low
 473 or null landslide susceptibility but in the central zone.
- 474 • Finally, Fig. 12e shows a detail of the western area of the Kyrgyz Republic, where a high landslide
 475 susceptibility is observed along the slopes adjacent to the river network.

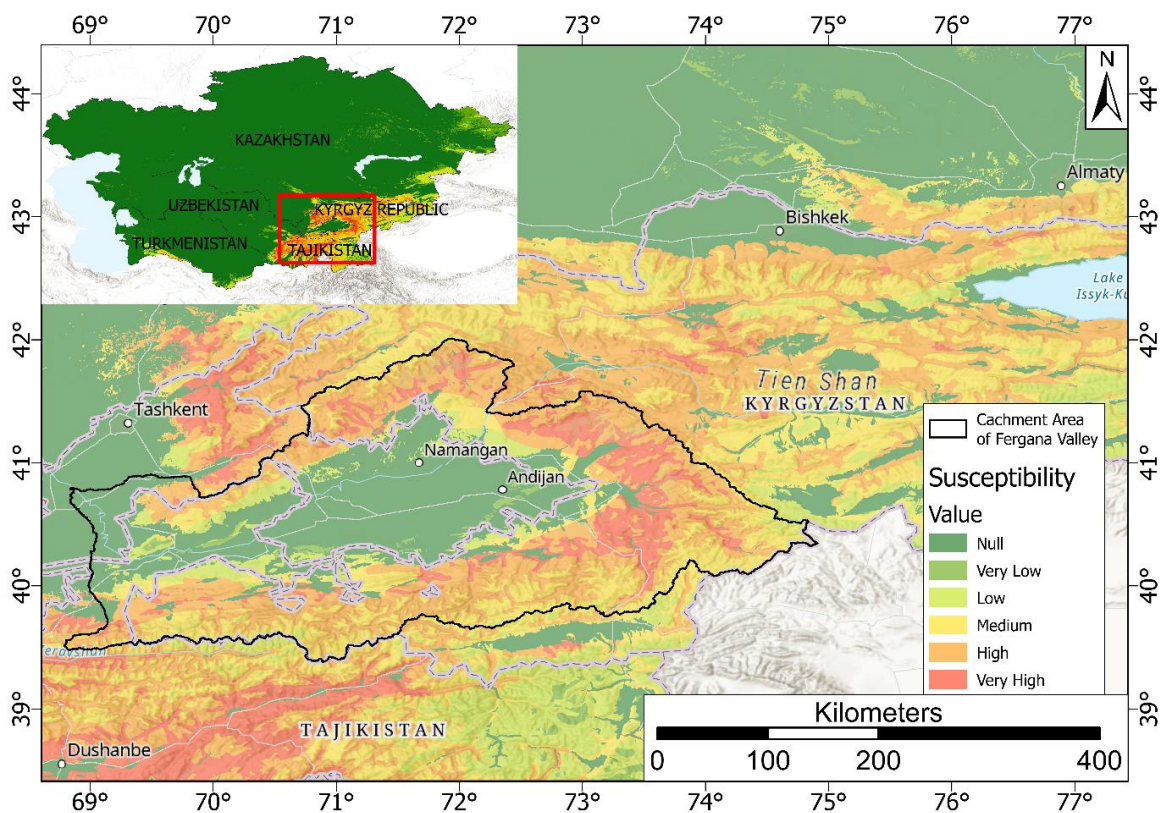


476

477 **Figure 12. Details of the landslide susceptibility map.** (a) the city of Denau, Uzbekistan; (b) the city of Ura-
 478 Tube, Tajikistan; (c) the city of Dushanbe, Kyrgyz Republic; (d) the Lake Issyk-Kul, Kyrgyz Republic; (e) the
 479 eastern area of the Kyrgyz Republic. Black polygons represent landslide areas from the adopted landslide
 480 inventories. Basemap source: Esri, USGS, NOAA.

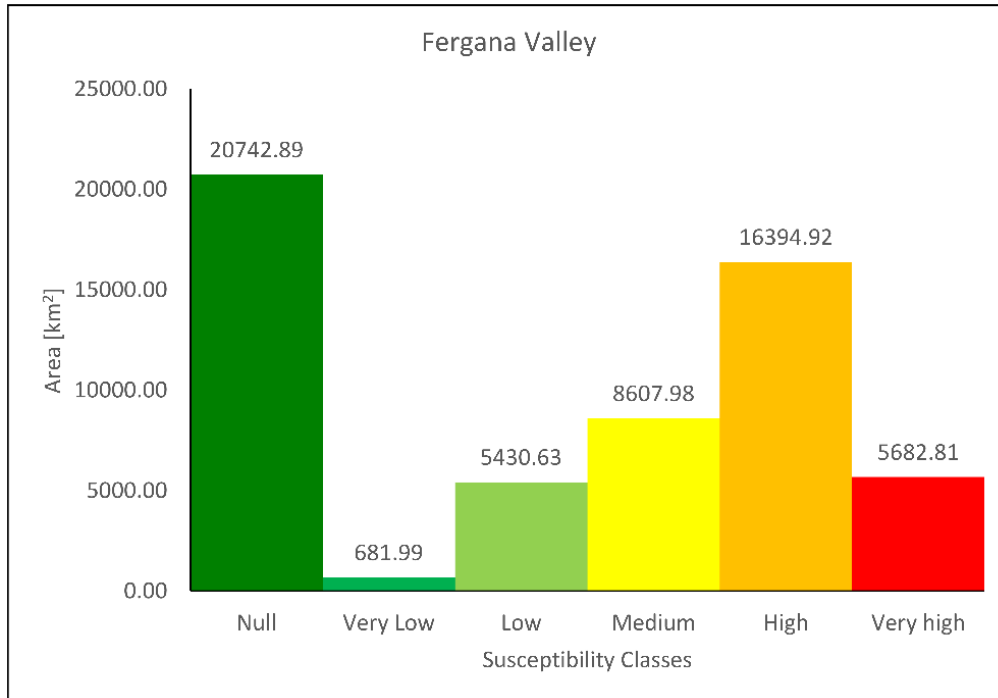
481 **4.2 The Fergana valley mountainous rim**

482 The Fergana valley spreads across eastern Uzbekistan, southern Kyrgyz Republic, and northern Tajikistan (Fig.
483 13). It is one of the largest intermountain depressions in Central Asia, located between the mountain systems of
484 the Chatkal-Kuraminsk ranges in the north and the Turkestan--Alai in the south. The two main rivers, the Naryn
485 and the Kara Darya, flow into the valley and unite forming the Syr Darya. In this area landslides represent one of
486 the major natural hazards due to their frequent (seasonal) occurrence across large areas: in fact, they are particularly
487 concentrated in a range of altitudes between 700 and 2000 m along the topographically rising rim below its
488 transition into higher mountainous terrain (Roessner et al., 2000; 2004; 2005; Behling et al., 2014; 2016). This
489 region is quite densely populated, and landslides lead almost every year to damage of settlements and infrastructure
490 and loss of human life (Schloegel et al., 2011; Piroton et al. 2020). In this area landslide activity is caused by
491 complex interactions between tectonic, geological, geomorphological and hydrometeorological factors (Havenith
492 et al., 2015a, b). In the Fergana valley rim mass movements are often characterized by deep and steep scarps,
493 mobilize weakly consolidated sediments of Tertiary or Quaternary age, including loess deposits (Piroton et al.,
494 2020). These kinds of landslides are particularly deadly, and can be triggered by a combination of long-term slope
495 destabilization factors (e.g., rainfall and snowmelt) and short-term triggers (Danneels et al., 2008). Slope landslide
496 susceptibility was analysed in this area using the previously mentioned methodologies. Fig. 13 shows the particular
497 about the landslide susceptibility map obtained for the Fergana Valley, while Fig. 14 reports the histogram of the
498 area occupied by each susceptibility class.



499 **Figure 13. Detail of the landslide susceptibility map obtained for the Fergana Valley.** Basemap source: Esri,
500 USGS, NOAA.
501

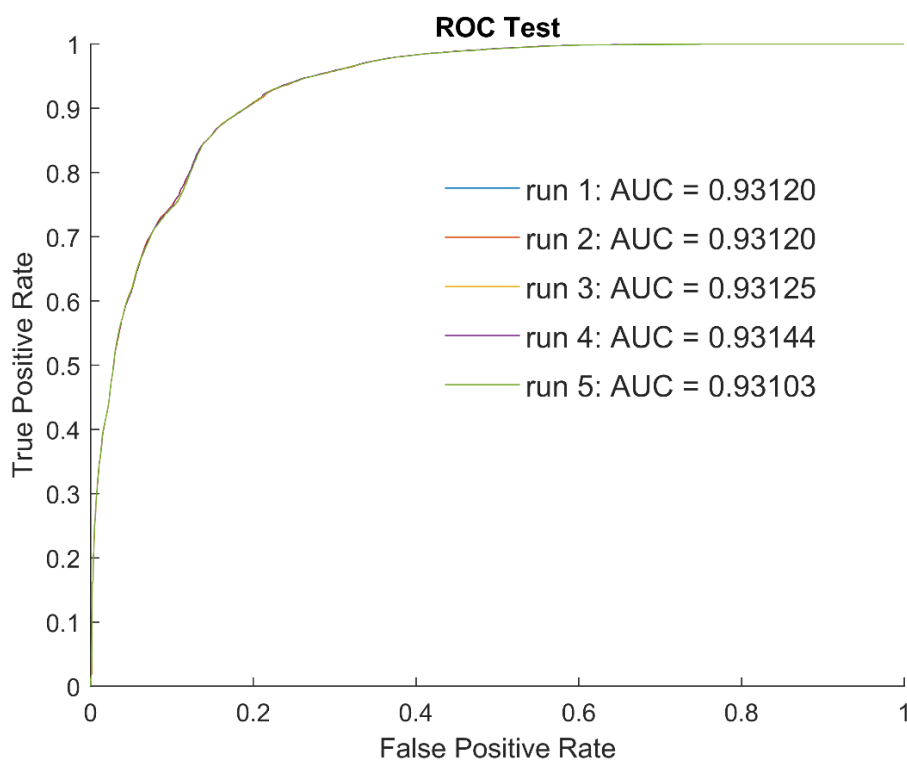
502 It can be observed that the most frequent susceptibility class in the Fergana Valley area is the Null class, which
 503 covers an area of about 20,743 km², that is 36% of the valley. The Very Low and Low classes occupy respectively
 504 an area of 681 km² (1.2%) and 5,431 km² (9.4%). The Medium class instead extends for about 8,608 km², namely
 505 the 15% of the total. The High class instead extends for about 16,395 km², that is 28.5% of the total and finally,
 506 the remaining 9.9% of the national territory, that is about 5,683 km², is classified in the Very High class.



507
 508 **Figure 14. Frequency histogram of susceptibility classes obtained for the Fergana Valley mountainous rim.**
 509 On each bar the corresponding area in km² is reported.

510 **4.3 Trained model performances and conditioning factors relevance**

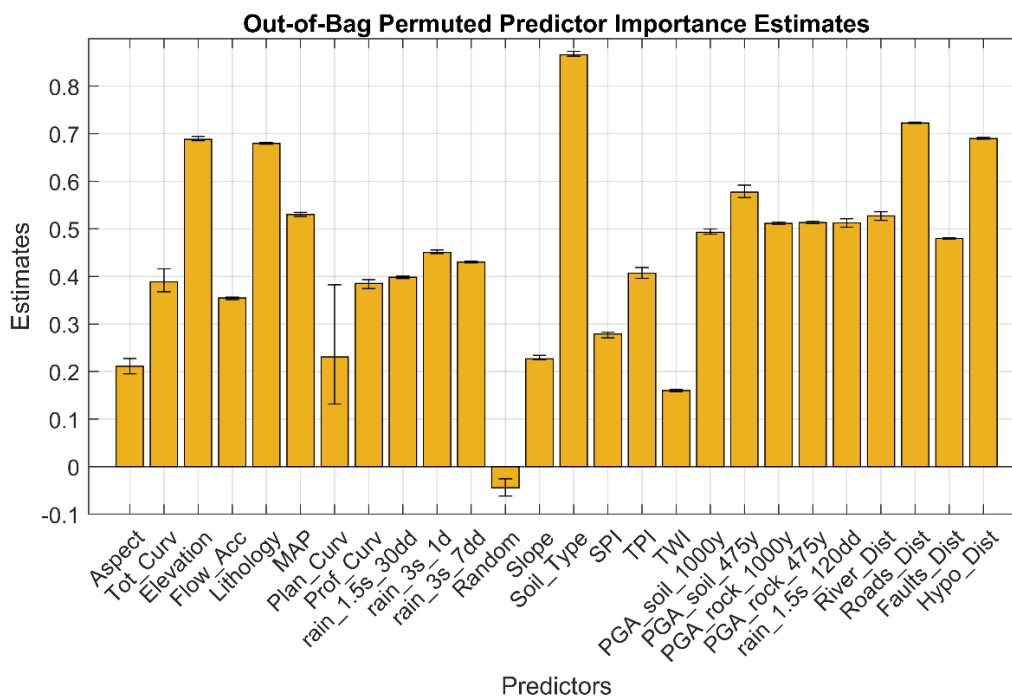
511 The RF was initially trained setting 1,000 trees to be growth. After the first run, the analysis of the out-of-bag error
 512 revealed that misclassification probability reduced significantly with a forest of 150 trees and then reduced slightly
 513 up to 500 trees, then it turned to be stable, so the optimal number of trees was set equal to 500 and used for all the
 514 simulations. As described above, the model was run 5 times to verify its stability and the AUC values ranged from
 515 0.93103 to 0.93144 (Fig. 15), with a mean value of 0.93122 and a standard deviation of 0.00015. The low variance
 516 of the AUC values confirmed the stability of the model and its applicability to the whole area. As we can see in
 517 the ranking of the susceptibility parameters, reported in Fig. 16, soil type, lithology, elevation, the distance from
 518 roads and hypocentres plays a crucial role in landslide susceptibility, since they are the five most influencing
 519 factors (for the four countries where the model was trained). Rainfall parameters are also important in the obtained
 520 landslide susceptibility, in particularly the 1-day rainfall value that shows the highest importance among the
 521 rainfall parameters. Also, the PGA maps are a relevant factor, while TWI and slope curvature are the less important
 522 parameters. The average AUC value of the models is 0.93122, indicating their very good quality. Such high AUC
 523 values can indicate the presence of overfitting issues, but this hypothesis can be discarded, since the random
 524 variable resulted without any importance in landslide susceptibility (negative OOB value).



525

526

Figure 15. ROC curve and relative AUC value for each model run (test samples).



527

528 **Figure 16. Variable importance in landslide susceptibility for the four countries where the model was**
 529 **trained.** From the 5 model runs, the results were averaged and displayed in this image, with the error bars showing
 530 the maximum and the minimum value obtained.

531 **5. Discussion**

532 The main issue affecting the used random forest model is the need of an adequate training dataset to properly
533 calibrate the predictor model. The first step of the work has been the homogenization of the landslide data, the
534 used landslide inventory was created starting from different sources, hence, with quite non-homogeneous (e.g., in
535 some cases the whole landslide perimeter was available, in other cases only a point representing the source area
536 of each landslide was provided, without info about the landslide dimension or propagation distance; more in
537 general there were few or no data about the landslide type or triggering causes). The lack of some data about the
538 landslides, or the partial or complete lack of landslides as in Kazakhstan and Turkmenistan, could lead to
539 underestimate the real landslide hazard of the studied countries, since some points could have been wrongly
540 classified (e.g., they have been considered as no landslide areas, but it was possible that a not reported landslide
541 was present). Furthermore, not all the adopted landslide inventories included information regarding the landslide
542 types, leading to the creation of a general landslide susceptibility map, where all the types of landslides are
543 considered. The created maps have been validated only using the available landslide dataset, providing good results
544 and highlighting the good prediction capability of the model. Anyway, an in-situ validation in some sample areas
545 can help to verify the quality of the results. As previously stated, for Turkmenistan there was no landslide inventory
546 available to train the RF model, therefore the corresponding LSM was obtained applying the model trained for the
547 other four countries. The lack of landslide data did not allow any validation of the result or estimation of the quality
548 of the susceptibility map of Turkmenistan. Furthermore, applying the model developed for the other countries, the
549 same importance of the conditioning factors (e.g., the independent variables) was assumed. For these reasons, the
550 landslide susceptibility map for Turkmenistan is more uncertain than those evaluated for the other four countries.
551 Among the used conditioning factors, soil type, distance from roads and distance from hypocentres resulted to be
552 the most influencing factors in slope stability, while planar curvature resulted with a high variability of its
553 importance. These parameters have been hence more deeply analysed to understand how they influence landslide
554 susceptibility. According to the partial dependency plots (Fig. 17), which show how the values of each
555 conditioning factor influence the landslide susceptibility, the soil types more related to landslides are lithosols and
556 cambisols, low thickness soils limited in depth by a continuous coherent and hard rock layer, located in steeply
557 slopes, with more than 30% of slope gradient. While the classes that have the lowest importance score are fluvisols
558 (young soils in alluvial deposits), xerosols (mainly arid clay) and chernozems (soils rich in organic matter), each
559 situated in flat to hilly areas, with less than 30% of slope gradient. Distance from roads, as expected, is important
560 for low values since the importance score is maximum for distance close to zero and it decrease exponentially with
561 the increasing of the distance. A similar behaviour can be noted with the distance from hypocentres, meaning that
562 areas close to hypocentres (within a radius of about 25 km) can more easily experience landslide phenomena in
563 case of future earthquakes. The partial dependency plot of planar curvature showed that the variability highlighted
564 in Fig. 16, is in fact, not so relevant since the range of the importance score is quite limited (values ranging from
565 0.4992 to 0.5008). In addition, it is possible noticing that negative values of planar curvature have a higher
566 importance score than zero values or positive values, meaning that concave slopes are more prone to landslide
567 than plain or convex surfaces.

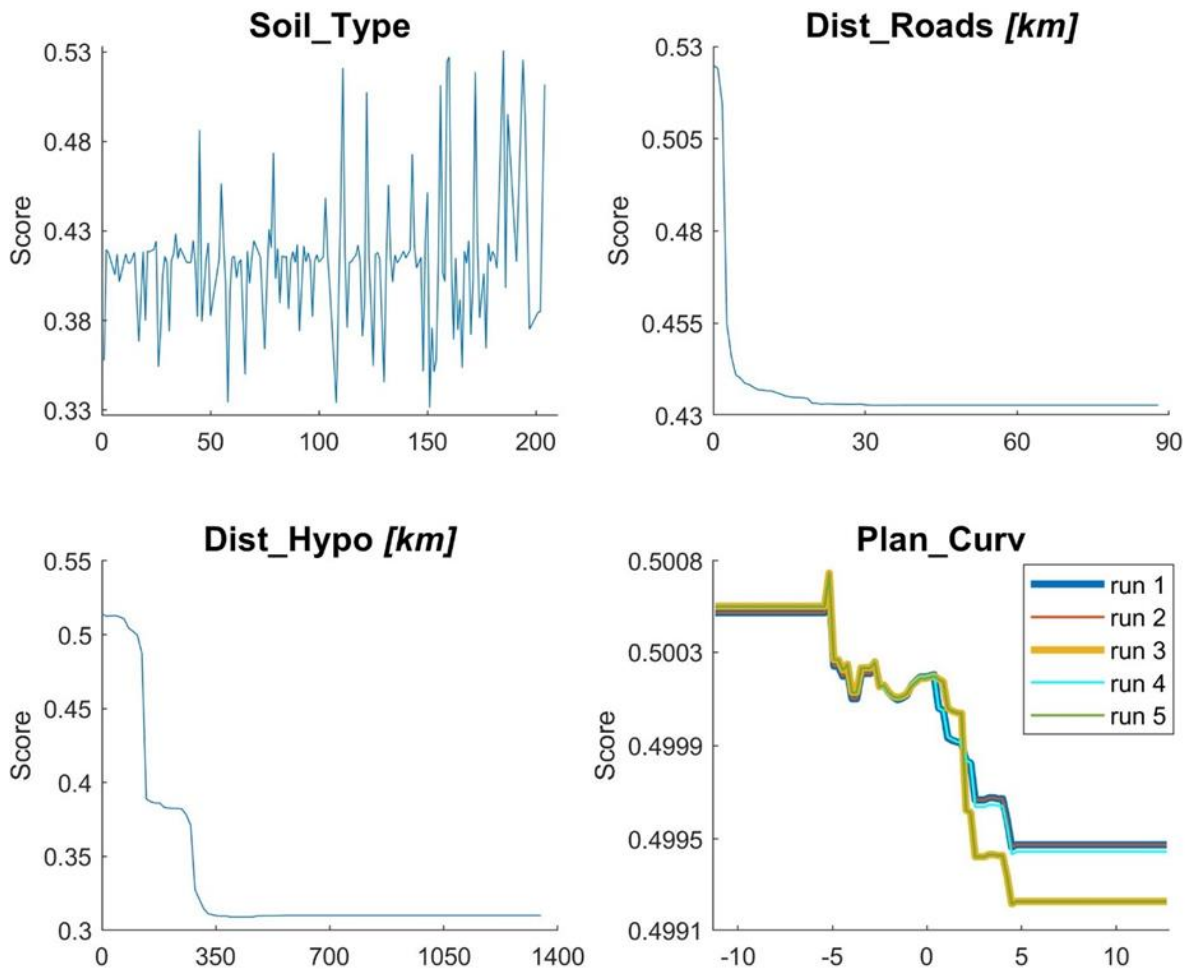


Figure 17. Partial dependence plots.

6. Conclusions

In this work a new landslide susceptibility assessment of Central Asia was carried out as a part of a multi-hazard approach in the framework of the SFRARR Project (“Strengthening Financial Resilience and Accelerating Risk Reduction in Central Asia”). Over 13,000 landslide elements were implemented in a Random Forest model to create a unique map in order to avoid boundary effects and obtain, a more homogeneous and with higher resolution susceptibility map with respect to previous works. The used approach allowed also to identify the most relevant landslides predisposing factors: soil type, distance from roads and hypocentres. The size and the heterogeneity of the study area required the use of many input variables (some of them never used before in landslide susceptibility assessment), and the elaboration of a high volume of data, as well as the adoption of specific procedures to account for the presence of heterogeneities and uncertainties in the input data (such as the presence of polygon and point landslides). The main limitation of the work is related to absence of data about type and geometry for several landslides; in the future a better input landslide inventory could help get to different susceptibility maps for different landslide types. Another limitation is due to the absence of any information about the presence or absence of landslides in Turkmenistan, which did not allow any clear validation of the results for this country.

584 The results provide a useful tool for landslide scientists, practitioners, and administrators involved in land use-
585 planning activities and risk reduction strategies in Central Asia.

586 **Code and data availability.** The landslide susceptibility model was implemented by using the cited landslide
587 inventory maps, published by the following authors: Behling et al., 2014, 2016, 2020; Havenith et al., 2015a;
588 Kirshbaum et al., 2015; Pittore et al., 2018; Strom and Abdrakhmatov, 2018. Other data implemented in the model,
589 such as MERIT DEM, geological formations, Active Fault Database, soil type map, rainfall maps are available
590 from Yamazaki et al. 2017, Persits et al., 1997, Styron and Pagani, 2020, <https://land.copernicus.eu/>,
591 www.ecmwf.int/en/forecasts/datasets/reanalysis-datasets/era5, respectively. The database on infrastructures, river
592 network, PGA and other landslide inventories were provided by the SFRAAR project partners: RED (Risk,
593 Engineering + Development – Pavia, Italy), OGS (National Institute of Oceanography and Experimental
594 Geophysics, Seismological Research Center, Trieste, Italy), IWPHE (Institute of Water problems, Hydropower,
595 Engineering and Ecology, Dushanbe, Republic of Tajikistan), ISASUZ (Institute of Seismology of the Academy
596 of Science of Uzbekistan, Tashkent, Uzbekistan) and the State Monitoring Service of the Republic of Uzbekistan
597 for tracking dangerous geological processes, LLP (Institute of Seismology of the Science Committee of the
598 Republic of Kazakhstan, Almaty).

599 **Author contribution.** Ascanio Rosi implemented the landslide susceptibility model, William Frodella conceived
600 with Ascanio Rosi the article structure and collected the data, Nicola Nocentini prepared the landslide
601 susceptibility data and supported the model implementation, Francesco Caleca prepared the infrastructure data for
602 the model implementation and performed the statistical analysis involving the landslide susceptibility areas and
603 the exposed elements. All the above-mentioned authors contributed to the writing of the article and the figure
604 graphics. Hans Balder Havenith and Alexander Strom provided the landslide databases from: i) Havenith, H.B.,
605 Strom, A., Torgoev, I., Torgoev, A., Lamair, L., Ischuk, A., Abdrakhmatov, K.: Tien Shan geohazards database:
606 Earthquakes and landslides. *Geomorphology* 249, 16–31, 2015a; and ii) Strom, A., Abdrakhmatov, K.: Rockslides
607 and rock avalanches of Central Asia: distribution, morphology, and internal structure. Elsevier, 441pg. ISBN: 978-
608 0-12-803204-6, 2018. They also provided the landslide pictures for figures 3 and 4, and critically reviewed the
609 paper. Veronica Tofani coordinated the work and reviewed the paper. Mirzo Saidov and Bimurzaev Gany
610 Amirgalievich provided the landslide databases of Tajikistan and part of Uzbekistan.

611 **Competing interests.** The contact author has declared that none of the authors has any competing interests.

612 **Acknowledgements.** This work was developed within World Bank-funded project “*Strengthening Financial*
613 *Resilience and Accelerating Risk Reduction in Central Asia*” (SFRARR), in collaboration with the European Union,
614 and the GFDRR (Global Facility for Disaster Reduction and Recovery), with the goal of improving financial
615 resilience and risk-informed investment planning in the central Asian countries (Kazakhstan, Kyrgyz Republic,
616 Tajikistan, Turkmenistan and Uzbekistan). This work represents the outcomes of the Task 7 “Landslide Scenario
617 Assessment”, coordinated by the UNESCO Chair on Prevention and Sustainable Management of Geo-
618 Hydrological Hazards (University of Florence). In particular, the authors would like to thank Gabriele Coccia and
619 Paola Ceresa from Red Risk Engineering (Pavia, Italy) for providing river network data and for the valuable
620 coordination and constant support, as well as Valerio Poggi and Chiara Scaini from OGS (National Institute of

621 Oceanography and Experimental Geophysics, Seismological Research Center, Trieste, Italy) for providing seismic
622 data (active faults, peak ground acceleration) and exposure data. We would also like to thank the partners from
623 Central Asia for the landslide data and fruitful collaboration, in particular: IWPHE (Tajikistan), ISASUZ and the
624 State Monitoring Service of the Republic of Uzbekistan for tracking dangerous geological processes (Uzbekistan),
625 the Institute of Seismology of the National Academy of Sciences of Kyrgyz Republic (ISNASKR), and Institute
626 of Seismology Limited Liability Partnership (LLP) of Kazakhstan.

627 **References**

- 628 Abdrakhmatov, K. Y., Aldazhanov, S. A., Hager, B. H., Hamburger, M. W., Herring, T. A., Kalabaev, K. B.,
629 Makarov, P. Molnar, S. V. Panasyuk, M. T. Prilepin, R. E. Reilinger, I. S. Sadybakasov, B. J. Souter, Yu. A.
630 Trapeznikov, V. Ye. Tsurkov Zubovich, A. V. Relatively recent construction of the Tien Shan inferred from
631 GPS measurements of present-day crustal deformation rates. *Nature*, 384(6608), 450-45319, 1996.
- 632 Abdrakhmatov, K., Havenith, H.B., Delvaux, D., Jongmans, D., Trefois, P.: Probabilistic PGA and Arias Intensity
633 Maps of Kyrgyz Republic (Central Asia). *J. Seismol.* 7.2: 203-220, 2003.
- 634 Akgun, A. A.: comparison of landslide susceptibility maps produced by logistic regression, multi-criteria decision,
635 and likelihood ratio methods: A case study at İzmir, Turkey. *Landslides*, 9, 93–106, 2012.
- 636 Bazzurro, P. et al.: Strengthening Financial Resilience and Accelerating Risk Reduction in Central Asia - the
637 SFRARR project. The SFRARR probabilistic flood hazard assessment. In prep. for the Special Issue
638 “Regionally consistent risk assessment for earthquakes and floods and selective landslide scenario analysis
639 in Central Asia”. *Natural Hazards and Earth System Sciences (NHES)*.
- 640 Behling, R., Roessner, S., Kaufmann, H., Kleinschmit, B.: Automated spatiotemporal landslide mapping over large
641 areas using rapideye time series data. *Remote Sens.* 6, 8026–8055, 2014.
- 642 Behling, R., Roessner, S., Golovko, D., Kleinschmit, B.: Derivation of long-term spatiotemporal landslide
643 activity—A multi-sensor time series approach. *Remote Sens. Environ.* 186, 88–104, 2016.
- 644 Behling, R., Roessner, S.: Multi-temporal landslide inventory for a study area in Southern Kyrgyz Republic
645 derived from RapidEye satellite time series data (2009 – 2013). V. 1.0. GFZ Data Services.
646 <https://doi.org/10.5880/GFZ.1.4.2020.001>, 2020.
- 647 Brabb, E.E.: Innovative approaches to landslide hazard mapping, in: *Proceedings 4th International Symposium on*
648 *Landslides*, Toronto, 1, 307–324, 1984.
- 649 Breiman, L.: Random forests. *Mach. Learn.* 45, 5–32, 2001.
- 650 Brenning, A.: Spatial prediction models for landslide hazards: Review, comparison and evaluation. *Nat. Hazard*
651 *Earth Syst.* 5, 853–862, 2005.
- 652 CAC DRMI: Risk assessment for Central Asia and Caucasus: desk study review, 2009.
- 653 Carrara, A.: Multivariate models for landslide hazard evaluation. *J. Int. Assoc. Math. Geol.* 15, 403–426, 1983.
- 654 Cascini, L.: Applicability of landslide susceptibility and hazard zoning at different scales. *Eng. Geol.*, 102 (3-

655 4):164–177, 2008.

656 Catani, F., Lagomarsino, D., Segoni, S., Tofani, V.: Landslide susceptibility estimation by random forests
657 technique: sensitivity and scaling issues. *Nat. Hazards Earth Syst. Sci.* 13, 2815, 2013.

658 Chedia, O.K., Lemzin, I.N.: Seismogenerating faults of the Chatkal depression. In: *Seismotectonics and seismicity
659 of the Tien Shan*. Frunze, Ilim, 18–28, 1980.

660 Chen, L., Van Westen, C.J., Hussin, H., Ciurean, R.L., Turkington, T., Chavarro-Rincon, D., Shrestha, D.P.:
661 Integrating expert opinion with modelling for quantitative multi-hazard risk assessment in the Eastern Italian
662 Alps. *Geomorphology*, 273 (15):150–167, 2016.

663 Coccia, G. et al.: The SFRARR probabilistic flood hazard assessment. In prep. for the Special Issue “Regionally
664 consistent risk assessment for earthquakes and floods and selective landslide scenario analysis in Central
665 Asia”. *Natural Hazards and Earth System Sciences (NHES)*.

666 Corominas, J., Copons, R., Vilaplana, J.M., Altimir, J., Amigó, J.: Integrated landslide susceptibility analysis and
667 hazard assessment in the principality of Andorra. *Nat. Hazards*, 30 (3): 421–435, 2003.

668 Cruden, D.M., Varnes, D.J.: Landslide types and processes. *Landslides: Investigation and Mitigation*. Special
669 Report 247, Transportation Research Board, Washington, 36–75, 1996.

670 Danneels, G., Bourdeau, C., Torgoev, I., Havenith, H. B. Geophysical investigation and dynamic modelling of
671 unstable slopes: case-study of Kainama (Kyrgyzstan). *Geophysical Journal International*, 175(1), 17-34,
672 2008.

673 Delvaux, D., Abdrakhmatov, K.E., Lemzin, I.N., Strom, A.L.: Landslides and surface breaks of the 1911 Ms 8.2
674 Kemin earthquake, Kyrgyzstan, *Russian Geology and Geophysics*, 2001, 42, 10, 1667-1677, 2001.

675 Duman, T.Y., Can, T., Gokceoglu, C., Sonmez, H.: Application of logistic regression for landslide susceptibility
676 zoning of Cekmece Area, Istanbul, Turkey. *Environ. Geol*, 51, 241–256, 2006.

677 Ermini, L., Catani, F., Casagli, N.: Artificial Neural Networks applied to landslide susceptibility assessment.
678 *Geomorphology*, 66, 327–343, 2005.

679 European Commission Humanitarian Aid, Civil Protection, U.N.I.S. for D.R.R.: *Disaster Risk Reduction 20
680 Examples of Good Practice from Central Asia*, 2006.

681 Frattini, P., Crosta, G., Carrara, A.: Techniques for evaluating the performance of landslide susceptibility models.
682 *Engineering geology*, 111(1-4), 62-72, 2010.

683 GFDRR (Global Facility for Disaster Reduction and Recovery): *Disaster Risk Management Notes for Priority
684 Countries 2009-2015*. *Eur. Asia* 48–49, 2009.

685 GFDRR (Global Facility for Disaster Reduction and Recovery): *Europe and Central Asia-Country Risk Profiles
686 for Floods and Earthquakes*. 144 pg, 2016.

687 Goetz, J.N., Brenning, A., Petschkoc, H. Leopold P.: Evaluating machine learning and statistical prediction tech-
688 niques for landslide susceptibility modeling. *Comput Geosci.*, 81, 1-11, 2015.

- 689 Golovko, D., Roessner, S., Behling, R., Wetzel, H. U., Kleinschmidt, B: Development of multi-temporal landslide
690 inventory information system for southern Kyrgyz Republic using GIS and satellite remote sensing. PFG
691 2015, 157–172, 2015.
- 692 Havenith, H. B., Strom, A., Jongmans, D., Abdrakhmatov, A., Delvaux, D., Tréfois, P.: Seismic triggering of
693 landslides, Part A: Field evidence from the Northern Tien Shan. *Natural Hazards and Earth System Sciences*,
694 3(1/2), 135-149, 2003.
- 695 Havenith, H.B., Strom, A., Cacerez, F., Pirard, E.: Analysis of landslide susceptibility in the Suusamyр region,
696 Tien Shan: statistical and geotechnical approach. *Landslides* 3, 39–50, 2006a.
- 697 Havenith, H.B., Torgoev, I., Meleshko, A., Alioshin, Y., Torgoev, A., Danneels, G.: Landslides in the Mailuu-Suu
698 Valley, Kyrgyz Republic—hazards and impacts. *Landslides* 3, 137–147, 2006b.
- 699 Havenith, H.B., Strom, A., Torgoev, I., Torgoev, A., Lamair, L., Ischuk, A., Abdrakhmatov, K.: Tien Shan
700 geohazards database: Earthquakes and landslides. *Geomorphology* 249, 16–31, 2015a.
- 701 Havenith, H.B., Torgoev, A., Schlögel, R., Braun, A., Torgoev, I., Ischuk, A.: Tien Shan geohazards database:
702 Landslide susceptibility analysis. *Geomorphology* 249, 32–43, 2015b.
- 703 Havenith, H.B., Torgoev, A., Braun, A., Schlögel, R., Micu, M.: A new classification of earthquake-induced
704 landslide event sizes based on seismotectonic, topographic, climatic and geologic factors. *Geoenvironmental*
705 *Disasters*, 1(3), 1-24, 2016.
- 706 Havenith, H.B., Umaraliev, R., Schlögel, R., Torgoev, I., Ruslan, U., Schlogel, R., Torgoev, I.: Past and Potential
707 Future Socioeconomic Impacts of Environmental Hazards in Kyrgyz Republic. In *Kyrgyz Republic: Political,*
708 *Economic and Social Issues*; Olivier, A.P., Ed.; Nova Science Publishers, Inc.: Hauppauge, NY, USA; pp.
709 63–113, 2017.
- 710 Hong, Y., Adler, R., Huffman, G.: Use of satellite remote sensing data in the mapping of global landslide
711 susceptibility. *Nat. Hazards*, 43, 23–44, 2007.
- 712 Ishihara, K., Okusa, S., Oyagi, N., Ischuk, A.: Liquefaction-induced flow slide in the collapsible loess deposit in
713 Soviet Tajik. *Soils and foundations*, 30(4), 73-89, 1990.
- 714 Juliev, M., Pulatov, A., Hubl, J.: Natural hazards in mountain regions of Uzbekistan: A review of mass movement
715 processes in Tashkent province. *International Journal of Scientific & Engineering Research*, 8(2), 1102,
716 2017.
- 717 Kalmetieva, Z.A., Mikolaichuk, A. V, Moldobekov, B.D., Meleshko, A. V, Janaev, M.M., Zubovich, A. V.: Atlas
718 of earthquakes in Kyrgyz Republic. Central-Asian Institute for Applied Geosciences and United Nations
719 International Strategy for Disaster Reduction Secretariat Office in Central Asia, Bishkek, p 75, 2009.
- 720 Kirschbaum, D., Stanley, T., Zhou, Y.: Spatial and temporal analysis of a global landslide catalog. *Geomorphology*,
721 249, 4-15, 2015.
- 722 Lagomarsino, D., Tofani, V., Segoni, S., Catani, F., Casagli, N.: A tool for classification and regression using

723 random forest methodology: Applications to landslide susceptibility mapping and soil thickness modeling.
724 Environ. Model. Assess., 22, 201–214, 2017.

725 Lee, S.: Application of logistic regression model and its validation for landslide susceptibility mapping using GIS
726 and remote sensing data. Int. J. Remote Sens., 26, 1477–1491, 2005.

727 Li, F., Torgoev, I., Zaredinov, D., Li, M., Talipov, B., Belousova, A., Kunze, C., Schneider, P.: Influence of
728 Earthquakes on Landslide Susceptibility in a Seismic Prone Catchment in Central Asia. Appl. Sci, 11, 3768,
729 2021.

730 Manzo, G., Tofani, V., Segoni, S., Battistini, A., Catani, F.: GIS techniques for regional-scale landslide
731 susceptibility assessment: The Sicily (Italy) case study. Int. J. Geogr. Inf. Sci., 27, 1433–1452, 2013.

732 Martelloni, G., Segoni, S., Fanti, R., Catani, F.: Rainfall thresholds for the forecasting of landslide occurrence at
733 regional scale. Landslides, 9, 485-495, 2012.

734 Medeu, A.R., Blagovechshenskiy, A.R.: Seismogenic Landslide risk zoning in the surrounding areas of Almaty
735 city, Kazakhstan. Vestnick, 6, 121, 2016.

736 Molnar, P., Tapponnier, P.: Cenozoic Tectonics of Asia: Effects of a Continental Collision: Features of recent
737 continental tectonics in Asia can be interpreted as results of the India-Eurasia collision. science, 189(4201),
738 419-426, 1975.

739 Nadim, F., Kjekstad, O., Peduzzi, P., Herold, C., Jaedicke, C.: Global landslide and avalanche hotspots. Landslides,
740 3(2), 159-173, 2006.

741 Niyazov, R.A.: Landslides in Uzbekistan. FAN, Tashkent, 207 pp (in Russian), 2009.

742 Niyazov, R.A., Nurtaev, B.S.: Evaluation of Landslides in Uzbekistan Caused by the Joint Impact of Precipitation
743 and Deep-focus Pamir-Hindu Earthquakes. In Landslides: Global Risk Preparedness (pp. 253-265). Springer,
744 Berlin, Heidelberg, 2013.

745 Niyazov R.A.: Uzbekistan landslides. Uzbekistan landslide service. Technical report, 2020a.

746 Niyazov, R., Nurtaev, B., Bimurzaev, G., Tashpulatov, M.: Flow Slides in Uzbekistan: Overview and Case Studies.
747 In Workshop on World Landslide Forum (pp. 59-65). Springer, Cham, 2020b.

748 Pánek, T., Korup, O., Minár, J., Hradecký J.: Giant landslides and highstands of the Caspian Sea, Geology, 44
749 (11), 939–942, 2016.

750 Persits, F. M., Ulmishek, G. F., Steinshouer, D. W.: Maps showing geology, oil and gas fields and geologic
751 provinces of the Former Soviet Union (No. 97-470-E). US Geological Survey, 1997.

752 Piroton, V., Schlögel, R., Barbier, C., Havenith, H.B.: Monitoring the recent activity of landslides in the Mailuu-
753 suu valley (Kyrgyz Republic) using radar and optical remote sensing techniques. Geosciences, 10 (5), p. 164,
754 2020.

755 Pittore, M., Ozturk, U., Moldobekov, B., Saponaro, A.: EMCA Landslide catalog Central Asia. V. 1.0. GFZ Data
756 Services, 2018.

757 Poggi, V. et al. a.: Harmonising seismicity information in Central Asia: earthquake catalogue and faults. The
758 SFRARR probabilistic flood hazard assessment. In prep. for the Special Issue “Regionally consistent risk
759 assessment for earthquakes and floods and selective landslide scenario analysis in Central Asia”. *Natural
760 Hazards and Earth System Sciences (NHESS)*.

761 Poggi, V. et al. b.: Development of a state of art probabilistic seismic hazard model for Central Asia countries.
762 The SFRARR probabilistic flood hazard assessment. In prep. for the Special Issue “Regionally consistent
763 risk assessment for earthquakes and floods and selective landslide scenario analysis in Central Asia”. *Natural
764 Hazards and Earth System Sciences (NHESS)*.

765 Pollner, J., Kryspin-Watson, J., Nieuwejaar, S.: *Disaster Risk Management and Climate Change Adaptation in
766 Europe and Central Asia*. World Bank 1–53, 2010.

767 Pusch, C.: A comprehensive risk management framework for Europe and Central Asia. (No. 9). *Disaster Risk
768 Management Working Paper Series*, 2004.

769 Reichenbach, P., Rossi, M., Malamud, B.D., Mihir, M., Guzzetti, F.: A review of statistically-based landslide
770 susceptibility models. *Earth Sci. Rev.* 180, 60–91, 2018.

771 Roessner, S., Wetzel, H. U., Kaufmann, H., Kornus, W., Lehner, M., Reinartz, P., Mueller, R. *Landslide
772 Investigations in Southern Kyrgyz Republic Based on a Digital Elevation Model Derived from MOMS-2P
773 Data*. IAPRS, Vol. 33, Part B7, Amsterdam, pp. 1259 -1266, 2000.

774 Roessner, S., Wetzel, H.U., Kaufmann, H., Sarnagoev, A.: *Satellite Remote Sensing and GIS Based Analysis of
775 Large Landslides in Southern Kyrgyz Republic NATO Advanced Research Workshop: Security of Natural
776 and Artificial Rockslide Dams*”, Bishkek, Kyrgyz Republic 2004.

777 Roessner, S., Wetzel, H.U., Kaufmann, H., Sarnagoev, A.: *Potential of Satellite Remote Sensing and GIS for
778 Landslide Hazard Assessment in Southern Kyrgyz Republic (Central Asia)*”, *Natural Hazards*, Vol. 35, No.
779 3, pp. 395 -416, 2005.

780 Saponaro, A., Pilz, M., Wieland, M., Bindi, D., Moldobekov, B., Parolai, S., *Landslide susceptibility analysis in
781 data-scarce regions: the case of Kyrgyz Republic*. *Bull. Eng. Geol. Environ.* 74, 1117–1136, 2014.

782 Scaini, C. et al.: (in prep.) A new regionally consistent exposure database for Central Asia: population and
783 residential buildings. In prep. for the Special Issue “Regionally consistent risk assessment for earthquakes
784 and floods and selective landslide scenario analysis in Central Asia”. *Natural Hazards and Earth System
785 Sciences (NHESS)*.

786 Schiavina, M., Melchiorri, M., Pesaresi, M., Politis, P., Freire, S., Maffenini, L., Florio, P., Ehrlich, D., Goch, K.,
787 Tommasi, P., Kemper, T.: *GHSL Data Package*, Publications Office of the European Union, Luxembourg,
788 2022, ISBN 978-92-76-53071-8, JRC 129516, 2022.

789 Schlögel, R., Torgoev, I., De, Marneffe, C., Havenith, H.B.: Evidence of a changing size-frequency distribution
790 of landslides in the Kyrgyz Tien Shan, Central Asia. *Earth Surf Process Landf* 36(12), 1658– 1669, 2011.

791 Segoni, S., Tofani, V., Rosi, A., Catani, F. Casagli, N.: *Combination of rainfall thresholds and susceptibility maps*

792 for dynamic landslide hazard assessment at regional scale. *Front Earth Sci.*, 6 (85), 2018.

793 Stanley, T., Kirschbaum, D.B.: A heuristic approach to global landslide susceptibility mapping. *Nat. Hazards* 87,
794 145–164, 2017.

795 Sternberg R.: Damming a river: a changing perspective on altering nature. *Renewable Sustainable Energy Rev*
796 10:165–197, 2006.

797 Strom, A.L., Korup, O.: Extremely large rockslides and rock avalanches in the Tien Shan, Kyrgyz Republic.
798 *Landslides* 3, 125–136, 2006.

799 Strom, A.: Landslide dams in Central Asia region. *Journal of the Japan Landslide Society*, 47(6), 309–324, 2010.

800 Strom, A., Abdrakhmatov, K.: Large-Scale Rockslide Inventories: From the Kokomeran River Basin to the Entire
801 Central Asia Region (WCoE 2014–2017, IPL-106-2, in: *Workshop on World Landslide Forum*. Springer,
802 Cham, pp. 339–346, 2017.

803 Strom, A., Abdrakhmatov, K.: *Rockslides and rock avalanches of Central Asia: distribution, morphology, and*
804 *internal structure*. Elsevier, 441pg. ISBN: 978-0-12-803204-6, 2018.

805 Styron, R., Pagani, M.: The GEM Global Active Faults Database.” *Earthquake Spectra*, vol. 36, no. 1_suppl, Oct.
806 2020, pp. 160–180, 2020.

807 Tien Bui, D., Tuan, T. A., Klempe, H., Pradhan, B., Revhaug, I. Spatial prediction models for shallow landslide
808 hazards: a comparative assessment of the efficacy of support vector machines, artificial neural networks,
809 kernel logistic regression, and logistic model tree. *Landslides*, 13, 361–378, 2016.

810 Thurman, M.: *Natural Disaster Risks in Central Asia: A Synthesis*. UNDP BCPR, 2011.

811 Tiranti D., Nicolò G., Gaeta A. R.: Shallow landslides predisposing and triggering factors in developing a regional
812 early warning system. *Landslides* 16 (2): 235–251, 2019.

813 Trifonov, V.G., Makarov, V.I., Scobelev, S.F.: The Talas-Fergana active right-slip faults. *Ann Tectonicae* 6:224–
814 237, 1992.

815 Trigila, A., Frattini, P., Casagli, N., Catani, F., Crosta, G., Esposito, C., Spizzichino, D.: Landslide susceptibility
816 mapping at national scale: the Italian case study, in: *Landslide Science and Practice*. Springer, Berlin,
817 Heidelberg, pp. 287–295, 2013.

818 Ullah, S., Bindi, D., Pilz, M., Danciu, L., Weatherill, G., Zuccolo, E., . Anatoly Ischuk, A., Mikhailova, N.N.,
819 Abdrakhmatov, K., Parolai, S. Probabilistic seismic hazard assessment for Central Asia. *Annals of*
820 *Geophysics*, 58(1), 2015.

821 UN ISDR.: *Risk assessment for Central Asia and Caucasus: desk study review*, CAC DRMI 2009, Risk
822 Management Working Paper Series No. 9. The World Bank, 2009.

823 World Bank: *Natural Disaster Hotspots: Case Studies*. Disaster Risk Management Series No. 6, 2006.

824 World Bank: *Investigation and Analysis of Natural Hazard Impacts on Linear Infrastructure in Southern Kyrgyz*

825 Republic Desk and Field Studies Report. Report 68669, 2008.

826 World Bank: The Global Landslide Hazard Map: Final Project Report. Appendix A., 2020.

827 Yaning, C.: Landslide-debris flow and its prevention in Kazakhstan. *Arid Land Geography*, 1992.

828 Yamazaki, D., Ikeshima, D., Tawatari, R., Yamaguchi, T., O'Loughlin, F., Neal, J. C., Sampson, C.C., Kanae, S.,
829 Bates, P.D.: A high-accuracy map of global terrain elevations. *Geophysical Research Letters*, 44(11), 5844-
830 5853, 2017.

831 Yilmaz, I.: Landslide susceptibility mapping using frequency ratio, logistic regression, artificial neural networks
832 and their comparison: a case study from Kat landslides (Tokat—Turkey). *Computers & Geosciences*, 35 (6):
833 1125-1138, 2009.

834 Zubovich, A. V., Wang, X. Q., Scherba, Y. G., Schelochkov, G. G., Reilinger, R., Reigber, C., Mosienko, O.,
835 Molnar, P., Michajljow, W., Makarov, V.I., Li, J., Kuzikov, S.I., Herring, T.A., Hamburger, M.W., Hager
836 B.H., Dang, Y., Bragin, V.D., Beisenbaev, R.: GPS velocity field for the Tien Shan and surrounding regions.
837 *Tectonics*, 29(6), 2010.

838